Building Velocity Models for Steep-Dip Prestack Depth Migration through First Arrival Traveltime Tomography

Brooke J. Carney

Thesis submitted to the Faculty of the Virginia Polytechnic Institute and State University in partial fulfillment of the requirements for the degree of

Master of Science
in
Geophysics

Dr. John A. Hole, Chair

_____

Dr. Cahit Coruh

_____

Dr. Matthias Imhof

_____

November 20, 2000
Blacksburg, Virginia

Keywords: Refraction Tomography, Velocity Model Building, Prestack Depth Migration, Steep-dip Imaging

Building the Steep-dip Migration Velocity Model through First Arrival Traveltime Tomography

Brooke J. Carney

(ABSTRACT)

Although the petroleum industry has imaged reflections from the sides of salt domes, steeply dipping structures have not been imaged as reflectors outside of sedimentary basins; to do so requires appropriate data acquisition, prestack depth migration, and an excellent seismic velocity model. Poststack time migrated seismic images, normal moveout velocity analysis, well logs, and other geologic information are used to build the velocity model. In regions of interest outside of sedimentary basins, such as major strike-slip faults, seismic reflectivity is often sparse and little is known of detailed subsurface geology. Alternate methods of velocity model construction must be used. First arrival (refraction and turning ray) traveltime tomography is proposed to construct the preliminary velocity model for steep-dip prestack depth migration in settings with little a priori subsurface information. A densely spaced synthetic seismic data set with long-offset recording, modeled after a real survey across the San Andreas Fault, was constructed using a finite-difference algorithm. First arrival traveltimes were picked from the data and a velocity model was constructed using tomography. The velocity model was used to perform a Kirchhoff prestack depth migration of the synthetic shot gathers. The subsurface structure was sufficiently reconstructed that the velocity model could be refined through migration velocity analysis. A series of tomography tests was used to determine the spatial resolution limits of the velocity model. Isolated erroneous anomalies with sizes near the resolution limits were added to the velocity model derived from tomography and used as input for migration. This pessimistic test provided an adequate image and identifiable arrivals in migrated common image gathers, allowing the velocity model to be improved through migration moveout analysis. Data acquisition

requirements for tomography include long recording offsets and times, larger sources, and dense spacings, very similar to the requirements for steep-dip reflection imaging.

Grant and Funding Information

Funding for this research project has been provided by the National Science Foundation through grant # EAR-9909228. The Department of Geological Sciences of Virginia Tech has also aided in this research project through the Friend (Matthew J. Mikulich) Geophysics Fellowship and by providing teaching assistantships during my studies.

Author's Acknowledgments

I would like to thank Dr. John Hole for his insight and direction throughout this scientific process. He has aided me in gaining a tremendous amount of knowledge, but more importantly, he has shown me what it takes to be a true scientist. I would also like to thank my committee members, Dr. Cahit Coruh and Dr. Matthias Imhof for their opinions toward the betterment of the final result. Thanks goes to the many people in the Department of Geological Sciences who have helped me get things done in all my five years at school. Special thanks goes to Eric Wonderley and Mark Lemon, who have provided me with countless hours of computer support. Without the support and assistance of Connie Lowe, I would probably still be a senior undergraduate. Connie, thanks for everything you have done for me, but most importantly, thanks for being a friend when I needed you for things that had nothing to do with university. I would like to thank my wife, Jennifer L. Carney, for putting up with my high stress level for the last year; a lesser person would have given up on me. Her kind words of encouragement and her smiling face gave me a reason to fight on. A very special and heart felt Thank You goes to Rick and Vicky Carney, my parents, for instilling the values of courage and trust, and for making me believe that anything is possible if you just put your mind to it. Last, but definitely not least, a Thank You goes to my Lord and Savior Jesus Christ, for without him nothing is possible.

Table of Contents

INTRODUCTION

Prestack depth migration is essential to seismic reflection imaging in areas where steeply dipping structures or extreme lateral velocity variations exist in the subsurface, such as along the flanks of salt domes (Hale et al., 1992; McMechan et al., 1998) or in strike-slip fault zones (Lafond and Levander, 1995). Raypath distortions can be so severe in areas of complex velocity variations that conventional poststack processing often destroys reflection information (e.g., Shultz and Sherwood, 1980). To obtain a better quality image through depth migration, an accurate velocity model is required. However, the more complex the geology, the more difficult it is to find an accurate velocity model (Zelt et al., 1998; Lafond and Levander, 1993). There are many methods used in industry to construct velocity models for prestack depth migration, including interval velocity analysis (e.g. Mills et al., 1993), layer stripping techniques (e.g. Fagin, 1998), reflection tomography (e.g. Whiting, 1998), and beam stacking (e.g. Biondi, 1990). However, all of the different model building methods rely on an existing reflection image with a relatively high signal to noise ratio and continuous reflectors. Velocity information obtained from well logs and other *a priori* information is usually included in the model. While these methods provide a sufficient velocity model to produce a preliminary image, migration velocity analysis, including several iterations of depth migration, is usually needed to produce a final image (e.g. Van Trier, 1990; Tieman, 1995). Generally, these procedures provide satisfactory images in areas with good data quality, many wells, and *a priori* geologic information (e.g. Ratcliff et al., 1992). However, such information often does not exist in regions of geologic interest outside of sedimentary basins. Here, other methods of velocity model construction must be found.

First arrival (refraction) traveltime tomography is proposed as a method to construct a preliminary velocity model appropriate for prestack depth migration of steeply dipping structures. Similar to the approaches above, the preliminary velocity model can then be refined through migration velocity analysis. Tomography can be effective in regions of poor data quality or sparse reflectivity because refracted or turning first arrival energy is generally present and usually strong. A feasibility study is conducted to test the resolution of first arrival traveltime tomography for velocity model building and to show the effect of resolution limits on prestack depth migration. A

synthetic seismic data set with long-offset recording and densely spaced shots and receivers was constructed, based upon a real seismic survey across the San Andreas Fault (Rymer et al., 1999). Strike-slip fault zones in the crust often exhibit little coherent sub-horizontal reflectivity, have no well log or other subsurface geologic data, and contain large lateral and vertical velocity variations (e.g. Lemiszki and Brown, 1988); requiring prestack depth migration and alternate velocity model building techniques for a successful image.

GEOLOGIC SETTING

The geologic/tectonic structure of the Parkfield region of the San Andreas fault (SAF) is simple when compared to other portions of the San Andreas system. The fault is nearly linear, with only one major branch of seismic activity. However, at a detailed level, there is much complexity. The SAF separates two distinct geologic facies, The Salinian block to the West and the Franciscan assemblage to the East (Eberhart-Phillips and Michael, 1993). The Salinian terrane, to the West, is a plutonic arc complex that is locally overlain by a Miocene - Quaternary age, shallow sedimentary basin. This arc complex has been transported over 300 km Northwestward along the transform boundary. The Franciscan rocks to the East of the SAF are a predominantly sedimentary melange with more resistant rocks included. Both the Franciscan complex and the Mesozoic sedimentary basin to the West are highly deformed, providing for poor reflectivity on seismic reflection sections. However, the terrific amount of deformation has allowed fracturing of the basement Salinian granitoids, creating some internal reflectivity. Analogous to subhorizontal detachments imaged elsewhere, near-vertical faults, such as the San Andreas reflect seismic energy (Hole et al., 1996). In a crystalline setting, velocity variations across the fault zone can provide impedance contrasts necessary for reflection. To capture this reflection information, appropriate acquisition and processing parameters must be chosen.

VELOCITY MODEL AND SYNTHETIC SEISMIC DATA

A seismic velocity model was constructed that simulates a simplified geologic cross-section across the SAF, near Parkfield, California (Unsworth et al., 1997) (Figure 1). Young, highly deformed sediments overlie granitic rocks (Salinian) on the left side of

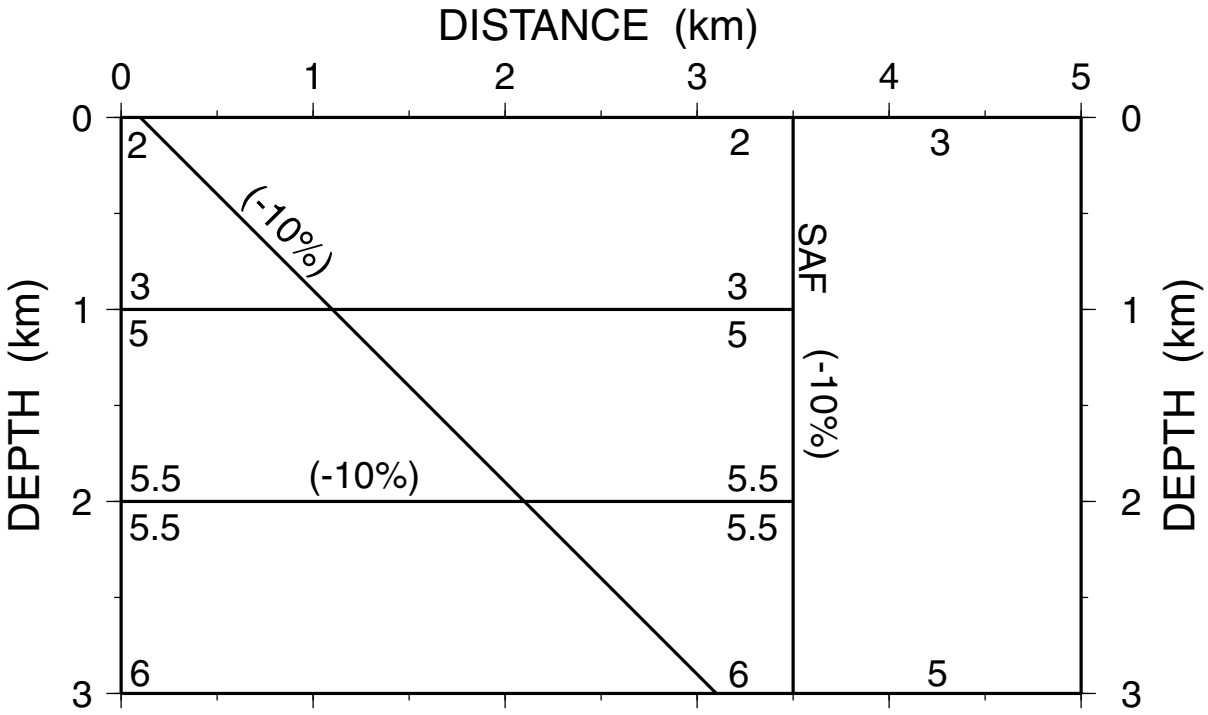

Figure 1. Velocity model used to create synthetic seismic data, designed after a real survey across the San Andreas Fault. Velocities are linearly interpolated between values (km/s) at the top and bottom of each block. Numbers in parentheses are velocity perturbations for low velocity zones with a thickness of about 15 m, represented by a solid line.

a vertical San Andreas fault, while low metamorphic grade sedimentary melange (Franciscan) exists on the right. Velocities to the left of the fault range from 2 km/s to 3 km/s in the sediments, are discontinuous at 1 km depth, and are 5 to 6 km/s in the basement. On the right side of the fault, a smooth gradient from 3 km/s at the surface to 5 km/s at 3 km depth simulates the sedimentary melange. A vertical low velocity zone, representing the San Andreas Fault, is located at X = 3.5 km. A simulated splay fault dipping 45^{o} towards the vertical fault and a horizontal detachment fault at 2 km depth are also represented by thin low velocity zones. All three zones contain velocities that are about 10% less than the surrounding velocities. The widths of the faults range from 1/8 to 1/3 wavelength of the dominant frequency (40 Hz) of the data to produce strong amplitudes through constructive interference. These low velocity zones mimic reflections in the crust, which are often caused by thin-bed layering rather than large-scale discontinuities.

Synthetic seismic data were created in this velocity model using a second order acoustic finite-difference wavefield propagation technique (Jensen et al., 1994). 98 shots were fired at a 50 m spacing. The line was a fixed spread of 490 receivers, placed every 10 m. The synthetic data is less dense than the real data set, which had a shot spacing of 10 m and a receiver spacing of 5 m (Rymer et al., 1999). Sparser data tests the effectiveness of refraction tomography by limiting the number of rays used to constrain the velocity model, partially compensating for the benefits of using noise-free data. The synthetic data include very long offsets, which are needed to constrain greater depths in refraction tomography. The synthetic wavelet was a zero-phase Ricker with a dominant recorded frequency of 40 Hz.

Several phases are of importance on the shot gathers (Figure 2). The direct first arrivals (phase A, including turning rays in the sediments) have a non-linear moveout away from the source location due to the vertical velocity gradient. They also have the largest amplitudes on the shot gathers. The horizontal sedimentary basement, at 1000 m depth, creates a reflection near 0.8 seconds, at zero offset (phase C). The 45^{o} dipping fault reflection intersects the first arrival at the fault's surface location and becomes parallel to the direct arrivals at long offsets (phase B). An additional, lower amplitude event exists at approximately 1.4 seconds, at zero offset (phase D) and is caused by the

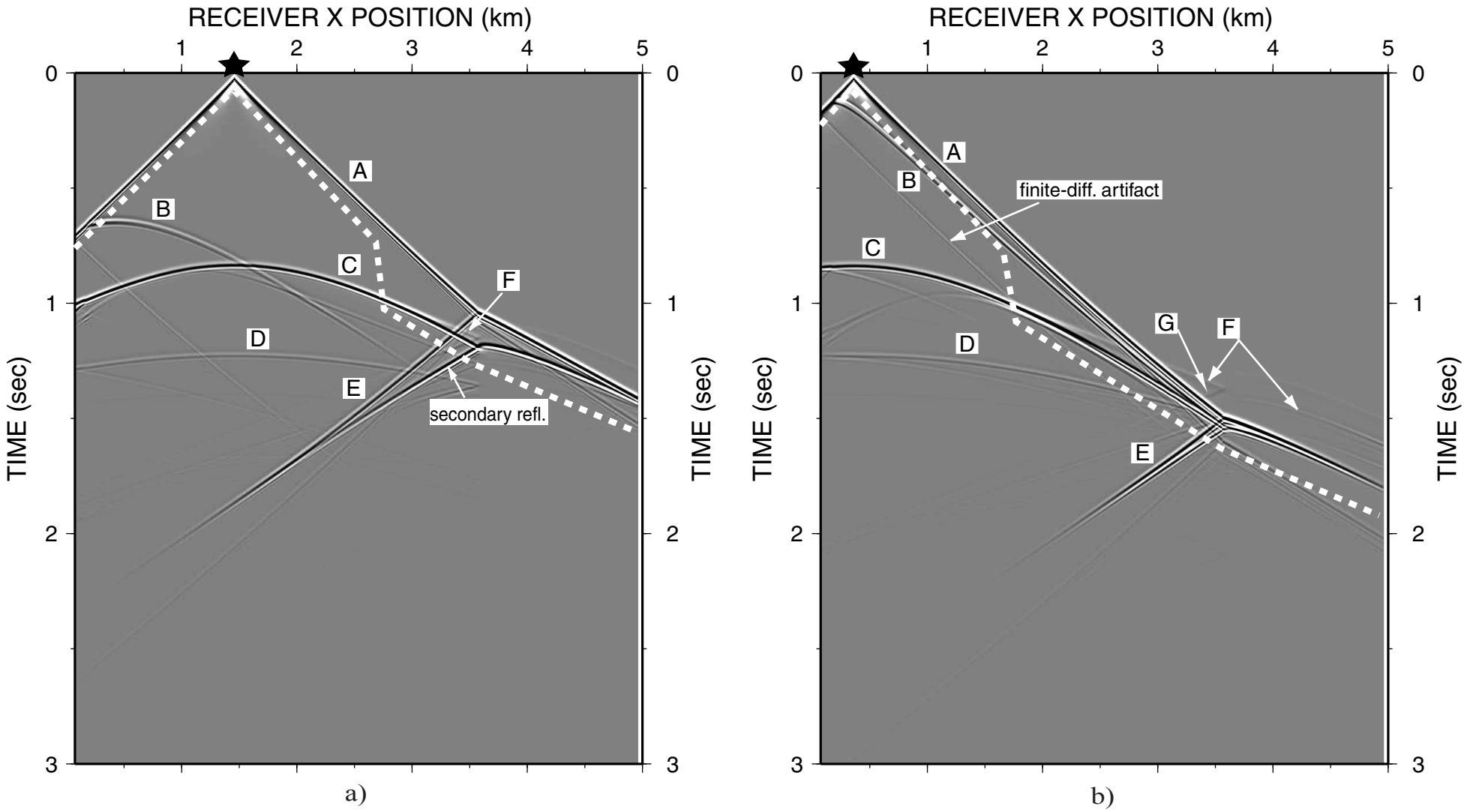

Figure 2. Synthetic shot gathers computed by acoustic finite-difference technique (Jensen et al., 1994) in the velocity model of Figure 1; 'A' are direct or turning ray arrivals within the sediments. 'B' is a reflection from the 45 degree dipping low velocity zone. 'C' is the reflection from the basement at 1 km depth. 'D' is the reflection from the low velocity zone at 2 km depth. 'E' is the turning ray reflection from the vertical fault. 'F' is the refraction from the 1 km basement interface. 'G' is the basment refraction reflected from the vertical fault. This smaller event 'G' is the first arrival reflection that is stacked properly in the migrated image. Stars indicate shot locations. The white dotted line indicates the top mute applied prior to migration, encompassing events 'A', 'F', and the post-critical part of 'C' on (b).

horizontal low velocity zone at 2000 m depth. The above three reflection events show a typical normal moveout on the shot gathers, while the reflection from the vertical fault displays a reversed moveout, with respect to the source point (phase E). This is explained by analyzing the geometry of the fault reflected raypaths (Figure 3) (Hale et al., 1992; Hole et al., 1996). The turning ray reflections from the upper 500 m of the fault arrive later in time towards the left, producing negative moveout. This non-typical moveout violates the assumption of normal moveout correction in traditional stack processing. A problem in first arrival traveltime migration is the presence of secondary arrivals, which do not stack properly in the migration (secondary refl. in Figure 2a). They will degrade the image unless stacked out via a high migration stack fold or by explicitly migrating their complex paths. Phase G in Figure 2b is the vertical fault reflected refraction that stacks in properly when using first arrival traveltimes in the migration, and is better explained below (Robinson, 1943).

KIRCHHOFF PRESTACK DEPTH MIGRATION

Kirchhoff migration (Schneider, 1978) is very flexible in dealing with large velocity contrasts and arbitrary dip angles and is computationally efficient, making it ideal for geologically complex areas such as the strike-slip San Andreas Fault (Zhuand et al., 1999). The technique used to calculate traveltimes is critically important to the success of the migration. We implemented a Kirchhoff prestack depth migration algorithm that uses first arrival traveltimes calculated using a finite-difference solution to the Eikonal equation (Vidale, 1990; Hole and Zelt, 1995). This forward modeling technique is useful since it is the same traveltime calculation algorithm that we used for tomography. The algorithm efficiently computes first-arrival times to all grid nodes within an arbitrarily complex velocity model. The one-way traveltime fields are calculated from both source and receiver through the entire velocity model. These two fields are then summed to obtain the two-way traveltime to all subsurface depth points. The amplitude at each time sample is applied to all image points with the same 2-way time. In effect, the energy has been smeared along equal 2-way traveltime paths for all samples. This is repeated for every trace and summed at each image point. Although the finite-difference code used to create the synthetic seismic data does account for amplitude information, the migration algorithm does not (Zhao et al., 1998). The

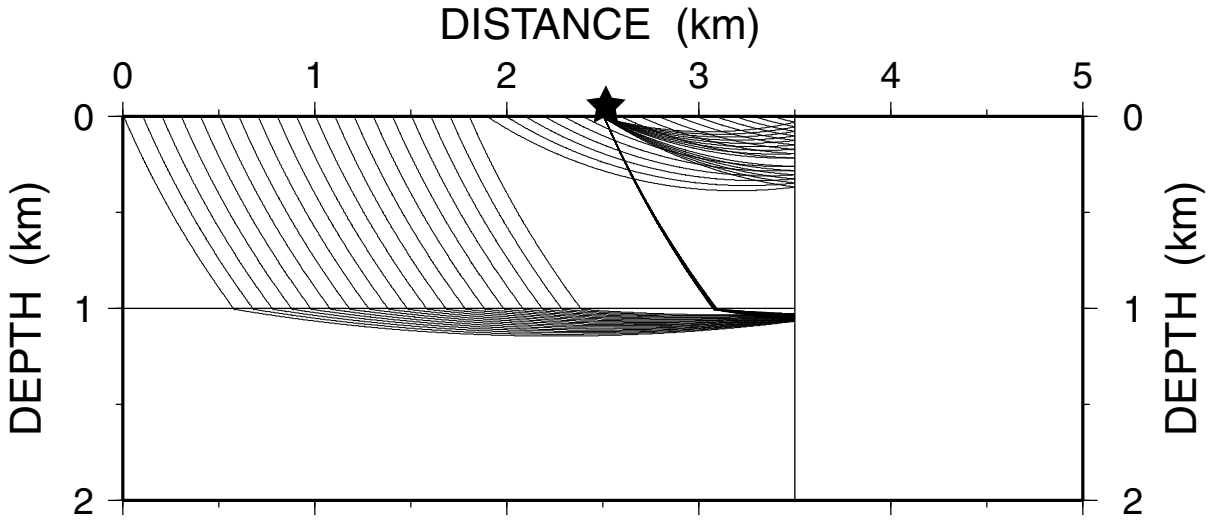

Figure 3. Reflected raypaths from vertical fault for shot indicated by star. Only rays that arrive first at every tenth receiver are shown. Maximum raypath reflection depth is around 1.2 km, indicating maximum imaging depth for vertical fault.

amplitude at a particular time sample is distributed uniformly to each image point with an equal two-way time, discounting true amplitude information that is present in the data.

Prior to migration, the shot gathers were muted to remove the first breaks and the post-critical portion of the 1 km reflection (Figure 2). The post-critical reflection, at greater than 1.5 km offset, introduced artifacts caused by the traveltime calculation technique of the migration code. Eikonal equation forward modeling techniques have a recognized problem with Kirchhoff depth migration if the reflected arrival of interest is a secondary arrival (Zhao et al, 1998; Geoltrain and Brac, 1998). One-way traveltimes are calculated from source to reflector and from receiver to reflector. If the true reflection time of an observed arrival and the computed time at some subsurface imaging point are different, then the reflection event will not be migrated to the correct position (Figure A1). The misplaced energy will stack out if fold is sufficient or will create an artifact in a low fold area. In general, when multiple raypaths exist from source to imaging point, the ray tracer can only trace one particular path for a particular arrival. This path may or may not be the desired one, because the orientation of the reflector is not known in advance. Ideally, every possible one-way ray is used in order to migrate all reflected events at the same imaging point. In practice, all Kirchhoff migration algorithms choose one ray. The ray chosen by Eikonal solvers is the first arrival. In the forward modeling algorithm, for the post-critical arrival from the 1 km boundary, the computed first arrival time from the source and receiver is for a ray that refracts along the basement. Since the ray along the basement is not the same as the ray that reflects from the basement, the times are different and the reflection energy is not properly migrated. This creates artifacts or missing information in the migrated image.

The 69 synthetic shot gathers to the left of the vertical fault were migrated using the true velocity model to obtain Figure 4. This image was used as a benchmark for further tests. Only shots to the left of the fault were used because an incorrect velocity model migrates left side and right side reflections from the vertical fault into different locations that may destructively interfere. In Figure 4, the 2 km reflector is well resolved in the center of the grid but fades to the left and right due to a lack of fold caused by limited array offsets and to an edge effect caused by the migration. The 45^{o} reflector is also clearly seen on the migrated image, between depths of 200 m and 2 km. The

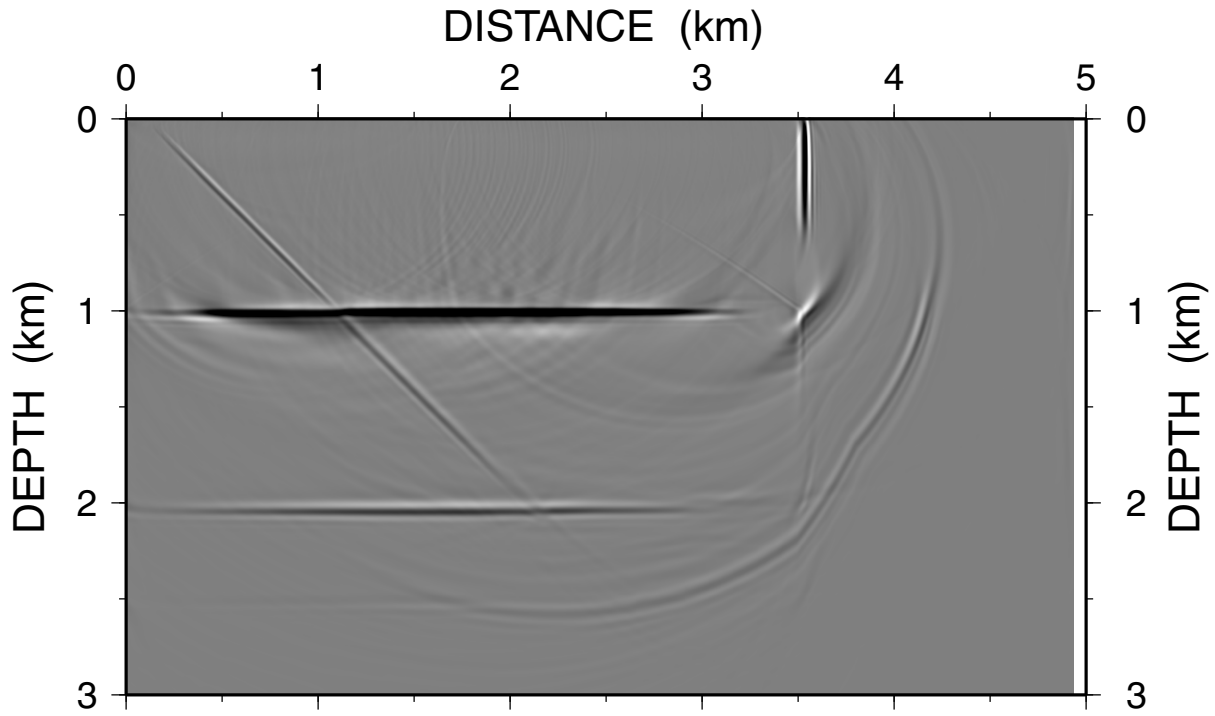

Figure 4. Migration image using true velocity model of figure 1. Horizontal reflections, the 45 degree fault reflection and the vertical San Andreas Fault are correctly located. Image degradation occurs near intersection of 1 km reflection and vertical fault reflection. Gray scale is used to avoid the problem of plotting steeply dipping and horizontal events together that occurs with traditional variable area or wiggle trace plots (Levin, 1998).

uppermost 200 m was muted along with the first arrivals. It is not imaged well below 2 km due to insufficient survey aperture for a 45^{o} dip at that depth. The 1 km horizontal reflector is well resolved, except for the left edge and the 200 m nearest the fault. This imaging problem is caused by a combination of low fold and a migration edge effect at the boundaries of the data (Figure A2, A3). The 200 m closest to the fault is further degraded by the forward modeling problem of refracted vs. reflected phases from above. The computed first arrival is actually a double refraction, first along the 1 km interface, and then along the vertical fault. While this is a valid ray, it is not a reflection. The energy is improperly located in the migrated image. A similar circumstance occurs for the vertical fault reflection, below a depth of 700 m. Below 700 m, the refracted phase from the sedimentary basement is the one-way first arrival to the vertical fault, instead of the raypath that lies within the sediments (Figure A4). This can be seen in Figure 5, which shows turning ray one-way first arrivals traveling in the sediments and then contacting the fault above 700 m depth. Deeper one-way first arrival raypaths refract into the basement on the left of the fault, then refract upwards along the vertical fault. The arcuate shaped artifact >= .5 km to the right of and below the vertical fault in the image is the artifact created from the turning ray reflections off of the vertical fault. Even though this reflection is one of the largest in amplitude on the shot gather (labeled E on Figure 2) its one-way path is a secondary arrival. The correctly migrated event for shots to the far left of the fault is event G in Figure 2, the reflected basement refraction beneath 1 km depth. In areas of highly variable velocities, these types of artifacts can be extremely detrimental to obtaining an acceptable migration image (Audebert et al., 1997).

TRAVELTIME TOMOGRAPHY

Traveltime tomography is a non-linear inversion technique that solves for an unknown velocity model from a data set of traveltimes (Bording et al., 1987). Calculated traveltimes through a known initial velocity model are compared to the picked traveltimes. Differences are used to perturb the starting velocity model so that it more closely approximates the true velocity model. The algorithm in this study (Hole, 1992) solves for the unknown velocities using a simple back-projection technique. First arrival raypaths are traced

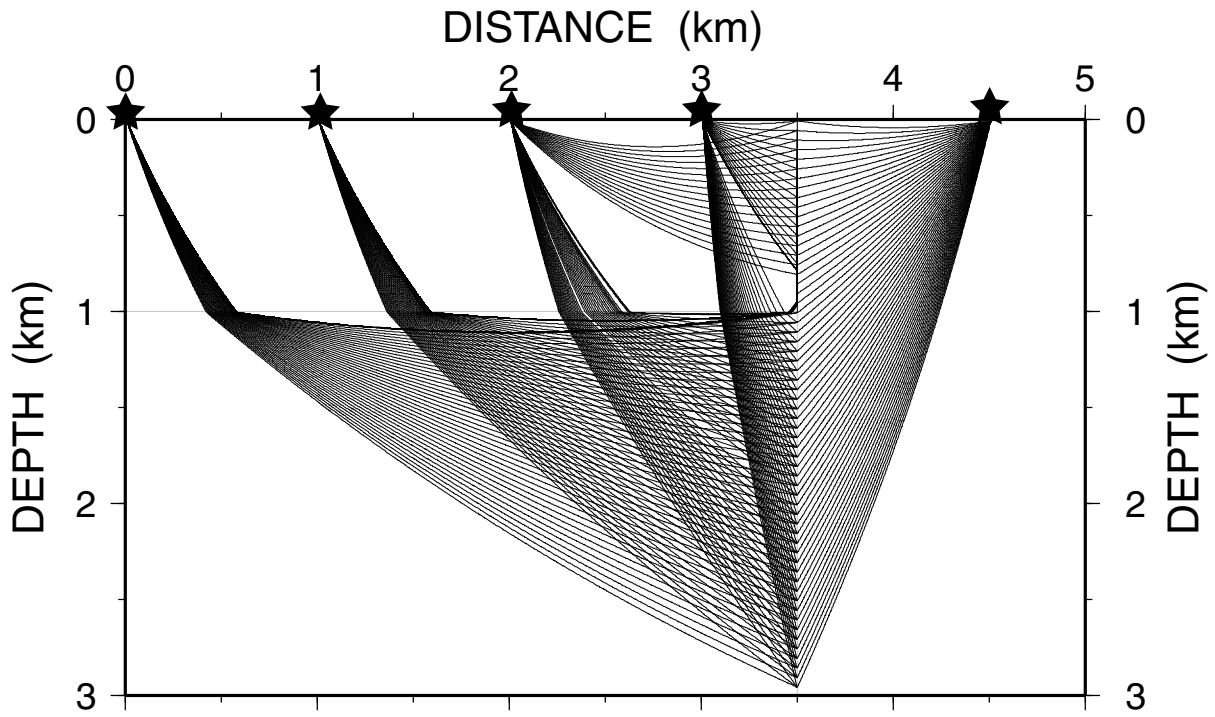

Figure 5. One-way first arrival raypaths from shots indicated by stars to regularly spaced points on the vertical fault. Points immediately above the 1 km basement on the fault appear to have no rays to any left side shots. The first arrival rays are plotted, but are refracted along the basement and fault. Such rays are used in the migration algorithm, but are inappropriate for imaging reflections from the fault.

through the reference velocity model using a finite-difference solution to the Eikonal equation (Vidale, 1990; Hole and Zelt, 1995). Differences in traveltimes of these raypaths from the picked traveltimes are used to update the velocity model by adding the velocity perturbations along each calculated raypath, from receiver to source. The subsurface is parameterized into equally spaced grid nodes having constant slowness values. A global smoothing operator is applied to the slowness (the reciprocal of velocity) perturbations after each iteration, and decreases in size with successive iterations, as the model converges. Large initial smoothing and slow convergence creates longer run-time for the inversion, but ensures a result with realistic values. This technique biases in favor of large-scale structures that are required by the data to exist in the final velocity model. Assuming sufficient ray coverage, the result is a smoothed version of the true subsurface structure, which is ideal for migration purposes (Lailly and Sinoquet, 1996).

The refraction subsurface ray coverage depends upon the subsurface velocity model and the data acquisition geometry. For a linear velocity function model, the maximum depth of ray coverage is a function of the surface velocity, the vertical velocity gradient, and the maximum offset (Stadtlander and Brown, 1997). The starting velocity model for the inversion usually is given an increasing velocity with depth so that initial raypaths return to the surface in accordance with Snell's Law. This increasing gradient provides the best approximation for the linearization assumption of the inversion. The velocity model in Figure 1 contains a vertical velocity gradient of 1 km/s in the sedimentary basin, which obeys the linearization formulation and allows the rays to turn back to the surface adding stability to the inversion (Figure 6). The starting velocity model is important for obtaining a final velocity model, in that it influences the non-unique portions of the model, both where rays exist and where they do not. If there is no seismic image or other subsurface information from which to draw geologic knowledge, then the starting model should contain minimum structure so as not to impose non-required structure on the final model. This approach, however, is not the only valid choice. A starting model that best approximates the believed true velocity model is sometimes used.

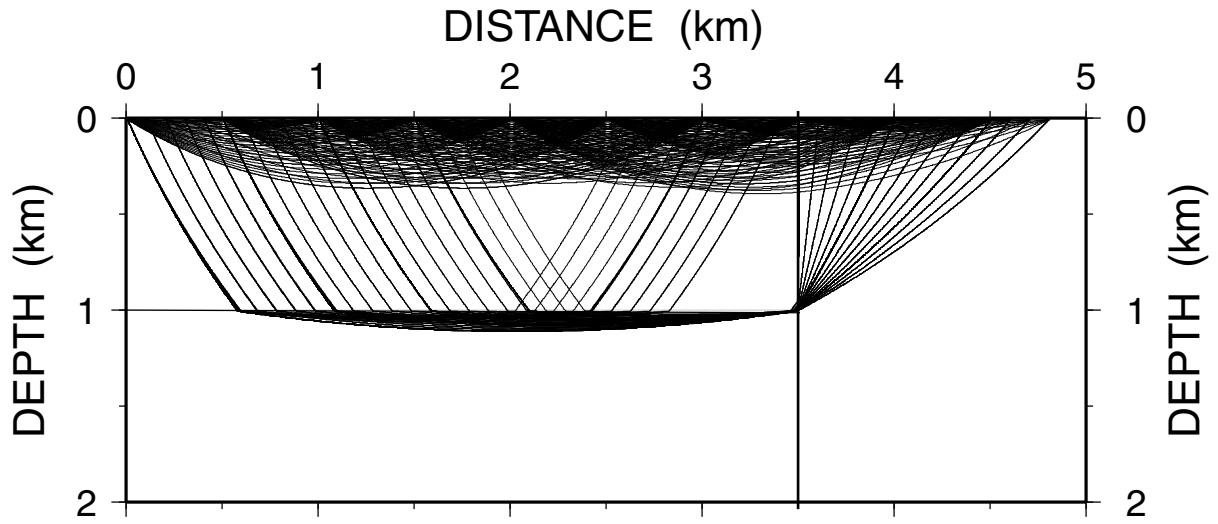

Figure 6. First arrival ray coverage through the velocity model of Figure 1. Only every tenth shot and tenth receiver are shown. Traveltimes along these raypaths are the input data for traveltime tomography. Regions between about 350 m depth and 1 km depth contain no first arrival turning rays. First arrival tomography can not recover subsurface velocity structure where no ray paths exist.

First arrival traveltimes were picked on all 98 shot gathers, including those on both sides of the fault, to obtain a data set for tomography. These first arrival raypaths are shown in Figure 6. Refraction rays are separated into a shallow set of rays and a deep set of rays according to the velocity gradient. To best simulate the case where nothing is known about the subsurface, a one-dimensional starting model was used with a linear velocity gradient from 2000 m/s at the surface to 6000 m/s at 3 km depth (Figure 7b). The starting smoothing operator size was very large, 3000 m horizontally and 1500 m vertically. This was done to provide stability in the least constrained portions of the model. Smaller smoothing sizes created artifacts in the model caused by too few data (rays) in the smaller areas. The smoothing aspect ratio was 2:1 to allow large lateral velocity changes. The smoothing size was decreased by 1/3 after every three iterations to a final size of 200 m horizontally and 100 m vertically.

The resulting velocity model (Figure 7) contains smoothly increasing velocities ranging from approximately 2000 m/s at the surface to 5300 m/s at 1.3 km depth on the left side of the fault. The right side of the fault contains velocities that range from 3000 m/s at the surface to 4000 m/s at about 1 km depth. This smoothly but accurately approximates the true velocity model, as shown in Figure 7b. The sharp vertical velocity contrast at the fault is recovered as a gradational boundary with a lateral extent of about 200 m in the shallow model and about 700 m in the deep model. This is due to the horizontally traveling rays not being able to resolve the exact location of the boundary, and to the applied smoothing. The boundary is sharpest in the shallow subsurface, corresponding to the area of denser ray turning ray coverage (Figure 6). The true velocity discontinuity at 1 km depth is not present in the tomography model, a result of the first arrival ray coverage and smooth tomography. The first arrival turning rays reach a maximum depth of approximately 350 m; while below this, refracted raypaths that turn in the higher velocity basement below 1 km are the first arrivals. This creates a shadow zone in the deeper portion of the sedimentary basin, between about 350m and 1 km in depth, within which no rays turn. The average velocity between these depths is constrained by the deeper rays. Tomography creates a smooth velocity gradient in this portion of the model, with velocities too high with respect to the true model in the deep sediments and too low in the upper basement (Figure 7b).

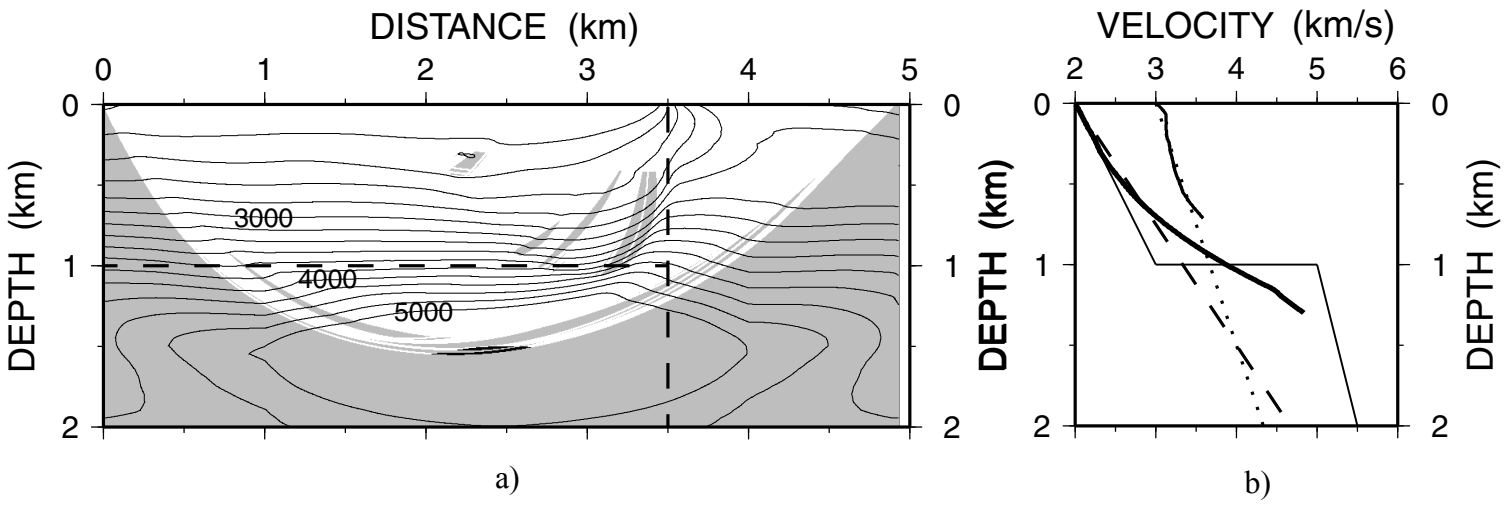

Figure 7. (a) Velocity model resulting from first-arrival traveltime tomography. The contour interval is 200 m/s. Regions more than 5 m from a ray are shaded gray. The edges and bottom portion of the model are unconstrained. (b) Vertical velocity profiles; thinnest black line is true velocity model at X = 2 km and dotted line is true velocity model at X = 4 km. Dashed line represents starting velocity model for tomography. Thickest black line represents velocity from tomography at X = 2 km, medium black line is velocity at X = 4 km. The latter lines end at base of ray coverage. The tomography velocity model is a smoothed image of the treu velocity model in Figure 1.

Alternate starting velocity models were tested. Velocity values were only slightly different than those in the model of Figure 7, existing in the unconstrained portions of the model below 1.4 km depth. Different smoothing aspect ratios were also used in some of the alternate tests. The 2:1 ratio was chosen (Figure 7), as it appeared to produce the best trade-off between vertical and horizontal resolution. However, in real data situations the best answer is rarely known in advance and thus, a slightly larger ratio of 3:1 or 4:1 is often utilized to better simulate raypath offset vs. depth ratios.

MIGRATION USING VELOCITY MODEL FROM TOMOGRAPHY

The tomographic velocity model (Figure 7) was used as the input for depth migration of the 69 shots to the left of the fault. The velocity model did an adequate job of reconstructing the subsurface structure, even after only one pass of migration (Figure 8). Remarkably, an acceptable velocity model was obtained even though the velocity model was built blindly, using a 1-D starting model that did not resemble the true velocity model, and only first arrivals were used. Reflectors are not as sharp when compared to the ideal model migration result, but can be readily identified for further velocity refinement using migration velocity analysis. This result could be due to the simple nature of the true velocity model, which will be tested and discussed below. The only portion of the image that was not adequately reconstructed was the same corner that created problems in the ideal case, which again is caused by the first arrival traveltime algorithm used in the migration. Unlike in the ideal case, the corner reflections are present but positioned deeper and to the right of their correct locations. These reflections stacked out in the real velocity model test, but now almost stack in, caused by smoothing the strong basement refractor. The smoothing allows fewer of the calculated one-way first arrival rays to be grabbed by the vertical fault and the 1 km basement, thus more of the turning ray reflections are first arrivals. The traced rays are now the preferred rays that travel within the basin, and not the low energy refracted rays. This is one argument for using a smooth velocity model in migration (Lailly and Sinoquet, 1996). The lower portion of the vertical fault and the rightmost portion of the 1 km reflector are smoothed into an arcuate shape that mimics the two-way traveltime field. The smooth inversion places a higher velocity to the left of the fault than actually exists, because higher

velocities to the right of the vertical fault and below the 1 km interface are being smoothed into the lower velocity basin. This causes the reflectors to shift to the right and deeper, since all shots were to the left side of the fault. Upon close inspection, the 1 km reflector is located at about 1050 meters depth and the 2 km reflector is located at about 2050 m depth. This shift in the reflector depths is caused by the previously described shadow zone phenomenon, which placed a higher velocity in the deep sedimentary basin. There is also some long-wavelength undulation in the horizontal reflectors at 1 km and 2 km depth caused by the lateral variations in the velocity model. The 45^{o} reflector is slightly misplaced, especially near the basement, again caused by the shadow zone in the ray coverage increasing the velocity near the 1 km interface (Figure 7).

Some minor deterioration of the image of the migrated horizontal reflectors occurs when using the velocity model from first-arrival traveltime tomography. However, the vertical fault reflector is only slightly altered from the migration with the true velocity model. It is properly imaged to about 600m depth, almost as deep as the 700m for the true model migration. A slight bend is present at the base of the dense first-arrival ray coverage. The vertical fault is better imaged than the horizontal events, which are traditionally easier to image. This is likely caused by migration ray paths being very similar to the tomography raypaths, and thus the average velocity along the paths is well constrained by tomography. In contrast, the tomography rays and the basement reflected rays are nearly perpendicular to one another, so average velocity in the horizontal direction at the 1 km interface is more subject to error and non-uniqueness.

EFFECT OF SYSTEMATIC PICKING ERRORS

First arrival traveltime picking of real data can be difficult due to noise, statics affecting trace-to-trace correlation, and emergent arrivals. In our synthetic data, refracted first arrivals at long offsets have much smaller amplitudes than the direct arrivals (Figure 2 phase F). This situation is common in refraction data wherever a strong refractor such as basement or the Moho, exists. On real data, the critically refracted phase could have been difficult to identify due to its small amplitude, and the more energetic direct arrival could have been picked erroneously as the first arrival in the presence of noise. A test was performed to determine the implications of making this error. Since the energetic

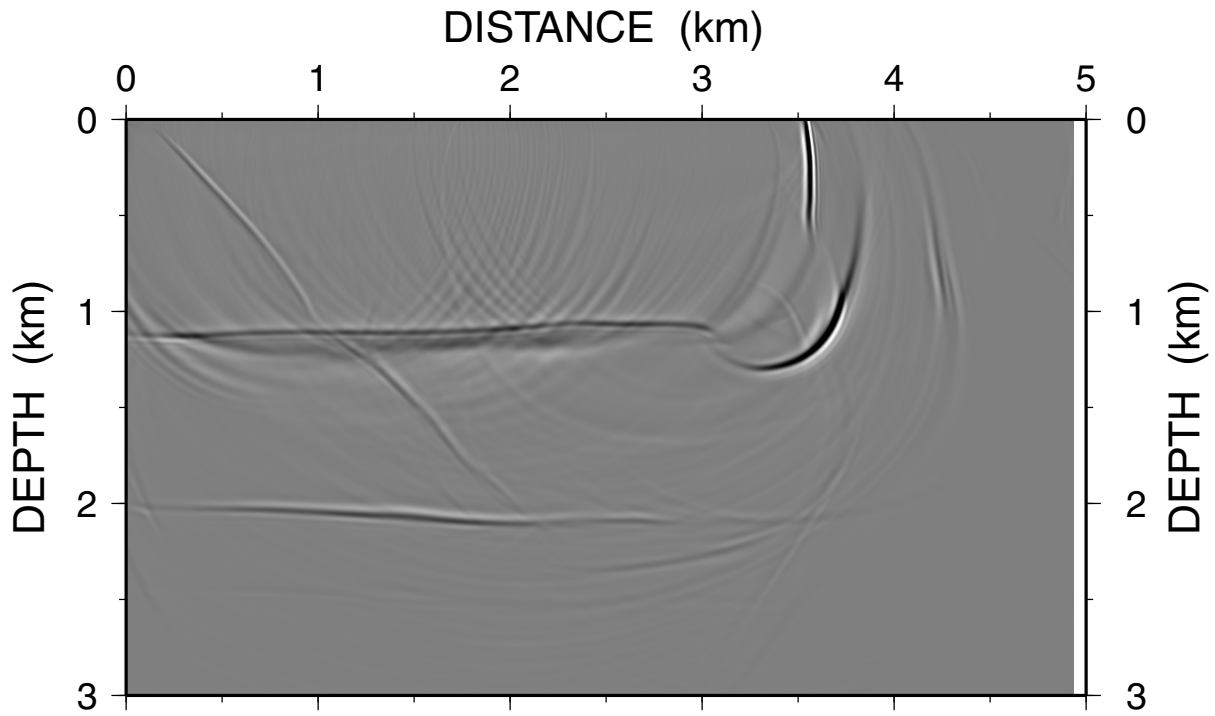

Figure 8. Migration image using velocity model of Figure 7a. The vertical fault is well imaged to 600 m depth. The 45 degree reflector is imaged to 1700 m depth with some errors near the 1 km interface caused by the shadow zone. The 1 km reflector is not as sharply defined as in Figure 4. The 2 km reflector is well imaged but varies mildly in depth. The gray amplitude scale is the same as that used in Figure 4.

events are direct waves that travel entirely within the sedimentary basin and sample to the base of the basin, picking these times would provide an accurate velocity model in the sediments but show no evidence of structure in the basement. To simulate the result of modeling these data, a velocity model is constructed having the same velocity as the true model (Figure 1) in the upper kilometer and constant low velocity below this.

Figure 9 is the migrated result from the velocity model that would be created using the more energetic secondary arrival. The basement and fault reflectors are perfectly imaged down to 1 km depth. The migration is no longer using the first arrivals traced in the true velocity model, but is using traveltimes computed for rays that travel entirely within the sediments. This is an acceptable image, in that it creates no false information about the subsurface and does overcome the first arrival disadvantage of the migration code, as both the tomography and the migration use the large amplitude phases within the sediments. However, it doesn't image the deeper subsurface as the deep velocity is very incorrect. Such a scheme of artificially altering the velocity model to migrate secondary arrivals has been suggested by Geoltrain and Brac (1998). A layer-stripping approach is an excellent method of building the velocity model, as it minimizes the error in the best-constrained parts of the model and then fixes these regions while deriving less-well constrained deeper regions (e.g. Zelt et al., 1992). In practice, identification of secondary arrivals is usually difficult. Incorporation of wide-angle reflection traveltimes in the tomography can improve the velocity model, but is difficult when near-vertical reflectivity is very weak. We limit our tests to first arrivals, as they are generally the easiest and most accurate to pick.

EFFECT OF SPATIAL RESOLUTION LIMITS

Small heterogeneities in the velocity field may not be resolved by tomography, and may cause misplacement of subsurface information during depth migrations. In relatively non-complex geologic provinces, this resolution limit is not of great concern, as a slightly smoothed version of the true model is ideal for migration (Lailly and Sinoquet, 1996). However, in areas of complex geology, resolution of subsurface structure is critical in obtaining an acceptable velocity model for prestack depth migration. To test the resolution limits of first-arrival traveltime tomography and to determine if these limits

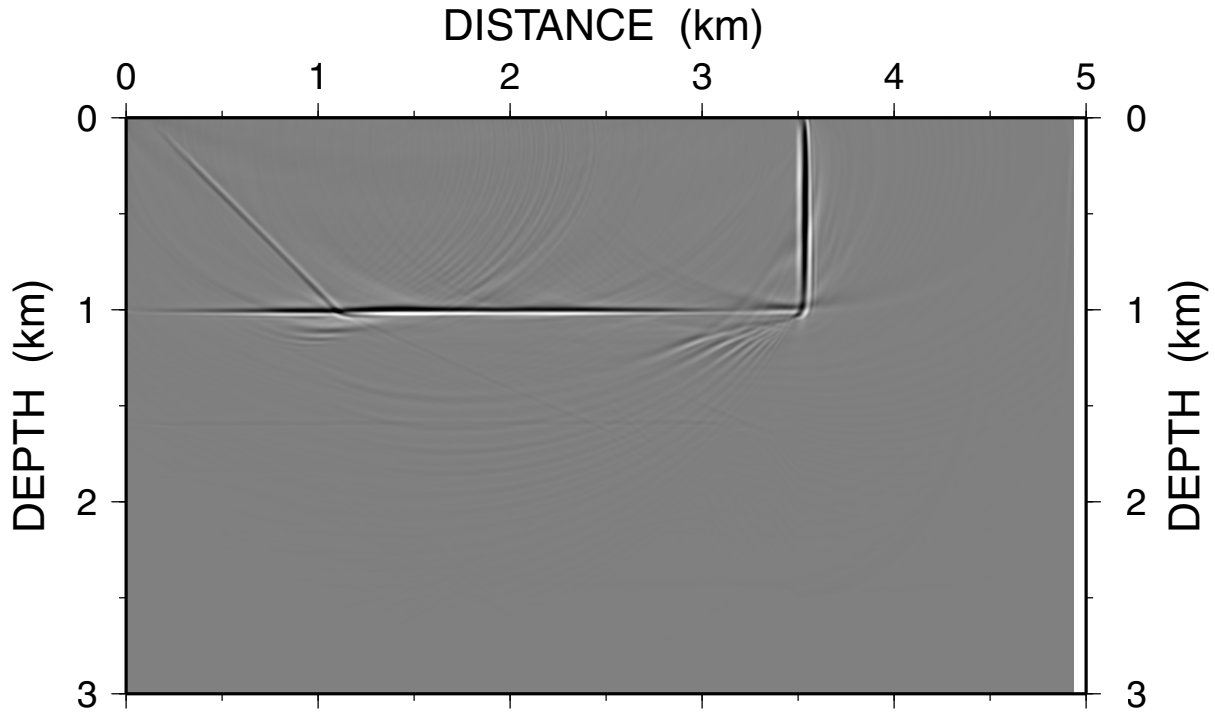

Figure 9. Migration image using true velocity model (Figure 1) in upper kilometer, and constant model at depth. This test simulates the velocity model that first-arrival traveltime tomography would produce if the stronger secondary arrival that turns in the basement is picked instead of the true first arrival. The vertical fault reflection, the 1 km reflector, and the 45 degree reflector are all well imaged in the upper 1 km. No deeper reflections are imaged due to incorrect velocities. The gray scale is the same as that used in Figure 4.

are sufficient for steep-dip pre-stack depth migration, several isolated anomaly tests were performed.

The velocity model of Figure 1 was used as a background model onto which isolated higher velocity bodies were added. Synthetic traveltimes were calculated in these velocity models using the finite-difference traveltime code (Vidale, 1990; Hole and Zelt, 1995). The anomalous velocity of 100 m/s for the added bodies was small enough so that there was little raypath relocation effect as compared to the background model. The anomalies were Gaussian in shape with a spatial standard deviation of 50-400 m. Separate tests were performed for determining the resolution in the shallow sediments (<400 m depth), the deeper sedimentary basin (>400 m depth), and in the shallow portion of the model to the right of the vertical fault. These synthetic traveltimes were inverted using the same tomography parameters as those used to construct the model in Figure 7. The velocity model of Figure 1 was used as the starting velocity model. The starting velocity model was subtracted from the tomography results to determine whether the anomalies were well resolved. Isolated anomalies were considered resolvable if they do not smear substantially from the original size. A reduction in anomaly amplitude was allowed. Use of the correct background velocity model tests the ideal resolution. More pessimistic tests were also conducted using the same 1-D starting model as above (Figure 7b) and the velocity model in Figure 7 subtracting the velocity model in Figure 7 from the results. This tests the complete non-linear resolution.

Two anomalies were placed at 150 m depth to test the portion of the model that is well constrained by dense first-arrival turning ray coverage (Figure 6). Large anomalies with a spatial standard deviation of 150 m were easily resolved, small ones (standard deviation of 50 m) were poorly resolved (Figure A5). Figure 10, showing anomalies of 100 m standard deviation, represents the approximate resolution limit. These anomalies were resolved fairly well in the vertical direction (about 1.5 times true size), but exhibited some smearing in the horizontal direction (about 3 times true size). The numerous turning rays passing through the anomalies in the horizontal direction allow the vertical dimension to be resolved (Figure 6). The smearing in the horizontal direction is a direct result of fewer vertical rays passing through the anomalies. The results of the more pessimistic test, using a 1-D starting model, shows that the anomalies are almost as well

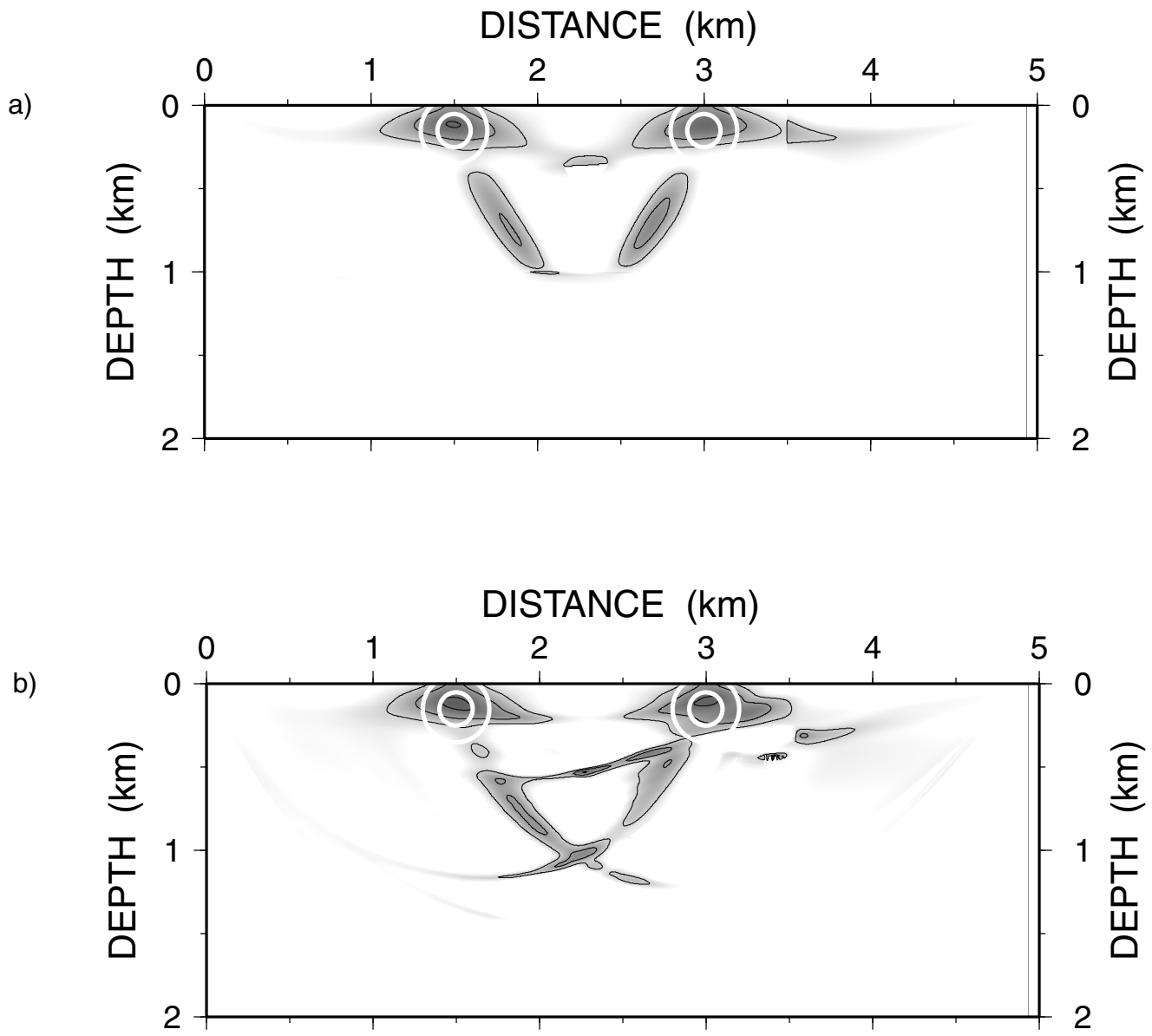

Figure 10. Resolution tests in the shallow portion of the model. Synthetic traveltime data were computed in a model consisting of Figure 1 plus two 100 m/s Gaussian-shaped high velocity bodies. White circles show one and two spatial standard deviation (100 m) locations for anomalies. (a) Tomography result using a starting model equal to Figure 1 and subtracting Figure 1 for the plot. (b) Tomography result using same starting model as Figure 7 (constant velocity gradient) and subtracting Figure 7a for the plot. The maximum imaged anomaly value is 32 m/s in a. and 34 m/s in b. and the contour interval is 8 m/s.

resolved as the ideal case in both the horizontal and vertical directions (Figure 10b). Most differences are in the deeper sediments and basement where the tomography does not well recover the background velocity model. This result confirms that an anomaly small in amplitude and spatial extent has an approximately linear effect on the tomography results.

To determine the resolution in the deep portion of the sedimentary basin where there is a shadow zone in first arrival turning ray coverage, anomalies were placed at 700 m depth (Figure 11). Anomalies of 100-300 m spatial standard deviation were tested and a 200 m standard deviation anomaly represents the approximate resolution limit. The results show that these anomalies were well resolved horizontally, but more poorly resolved parallel to the ray propagation direction at this depth. The 1-D starting model test shows substantially more smearing along the rays.

Anomalies of 50-150 m standard deviation were added to the right of the vertical fault to test the effect that errors in the velocity model on the right side would have on the migrated reflectors on the left side of the model. A 100 m spatial standard deviation anomaly was determined to be the approximate resolution limit (Figure 12). The anomaly is fairly well resolved near its top, but its base is smeared significantly. However, the anomaly has only a minor effect on the velocity model to the left of the fault. Thus, it has no effect on our steep-dip migrations, since only shots to the left of the fault were used in migration. A 1-D starting model test shows larger, but still minor smearing across the fault.

To test the effect of the resolution limits of first arrival time tomography on prestack depth migration, all five of the above anomalies, representing the largest structures that might not be resolved by tomography, were added to the tomography result in Figure 7. The effect of adding erroneous anomalies to the velocity model is similar to the effect of missing real anomalies. The amplitudes of the anomalies were increased from 100 m/s to 200 m/s. This test provides a pessimistic velocity model that might result from first-arrival tomography. The migrated image using this velocity model is shown in Figure 13. The 1 km and 2 km horizontal reflectors are of similar amplitude, but are undulatory, when compared to the migration result of Figure 8. However, the vertical fault reflection is less affected than the horizontal structures. It is

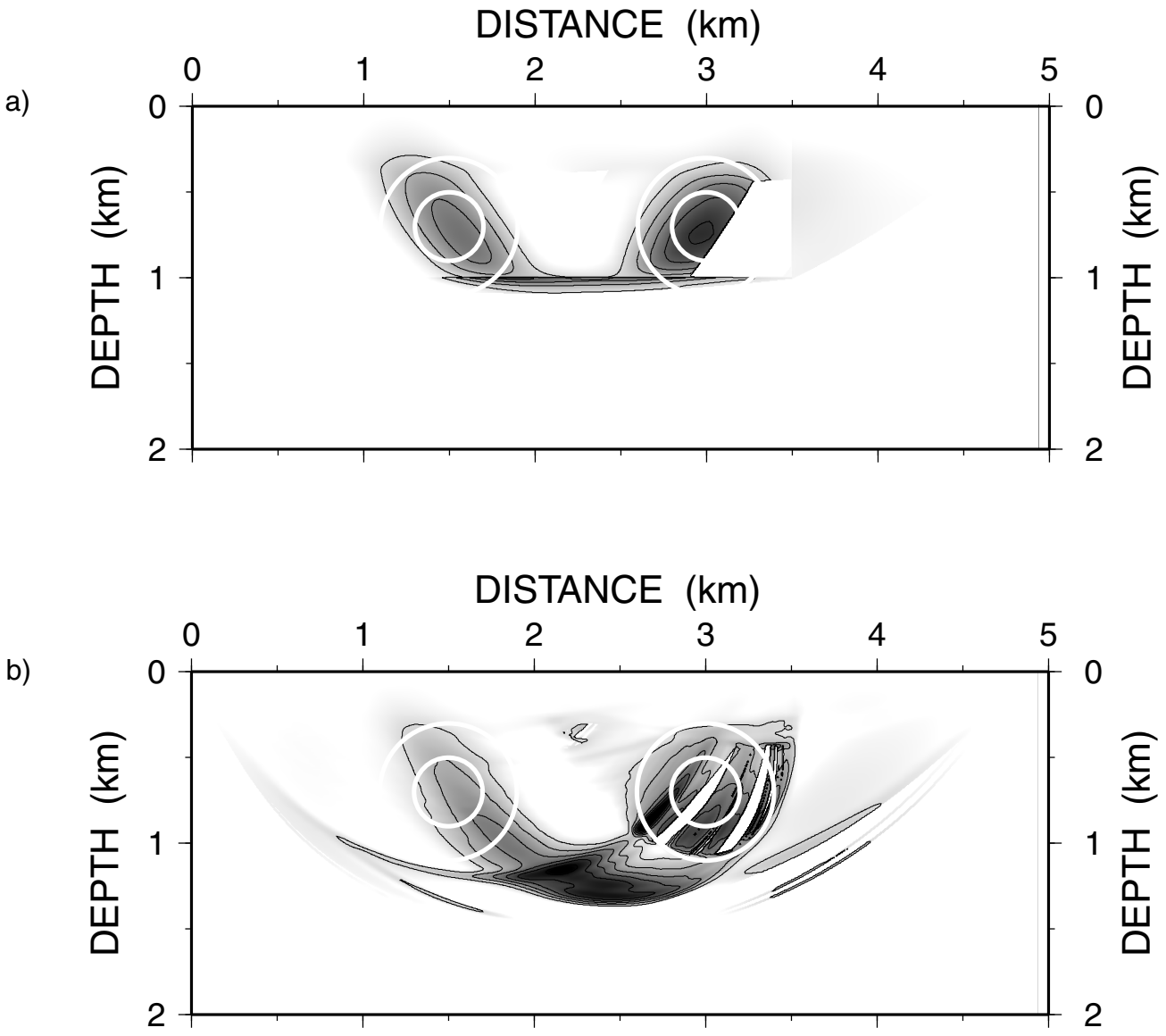

Figure 11. Plots similar to Figure 11, but for two 200 m spatial standard deviation anomalies at greater depths. (a) Tomography result using a starting model equal to Figure 1 and subtracting Figure 1 for the plot. (b) Tomography result using same starting model as Figure 7 (constant velocity gradient) and subtracting Figure 7 for the plot. The maximum anomaly value is 48 m/s in (a) and the contour interval is 8 m/s. White polygon cutting into right anomaly in (a) is where no rays penetrate. See Figure 6 for ray coverage.

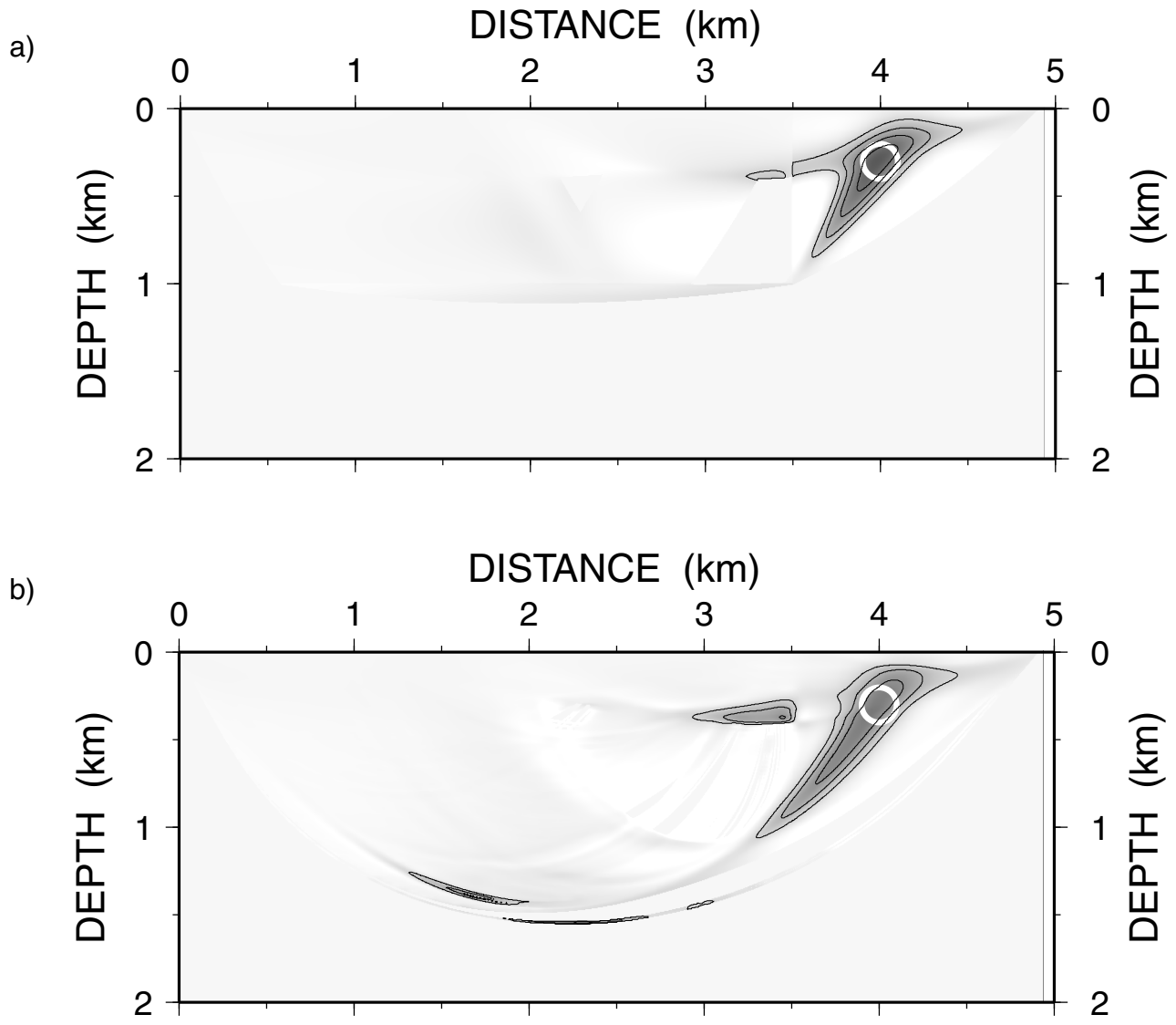

Figure 12. Plots similar to Figure 11, but for one 100 m standard deviation anomaly added to right side of vertical fault. (a) Tomography result using a starting model equal to Figure 1 and subtracting Figure 1 for the plot. (b) Tomography result using same starting model as Figure 7 (constant velocity gradient) and subtracting Figure 7 for the plot. The maximum velocity value is 18 m/s in (a) and 14 m/s in (b). The contour interval is 4 m/s.

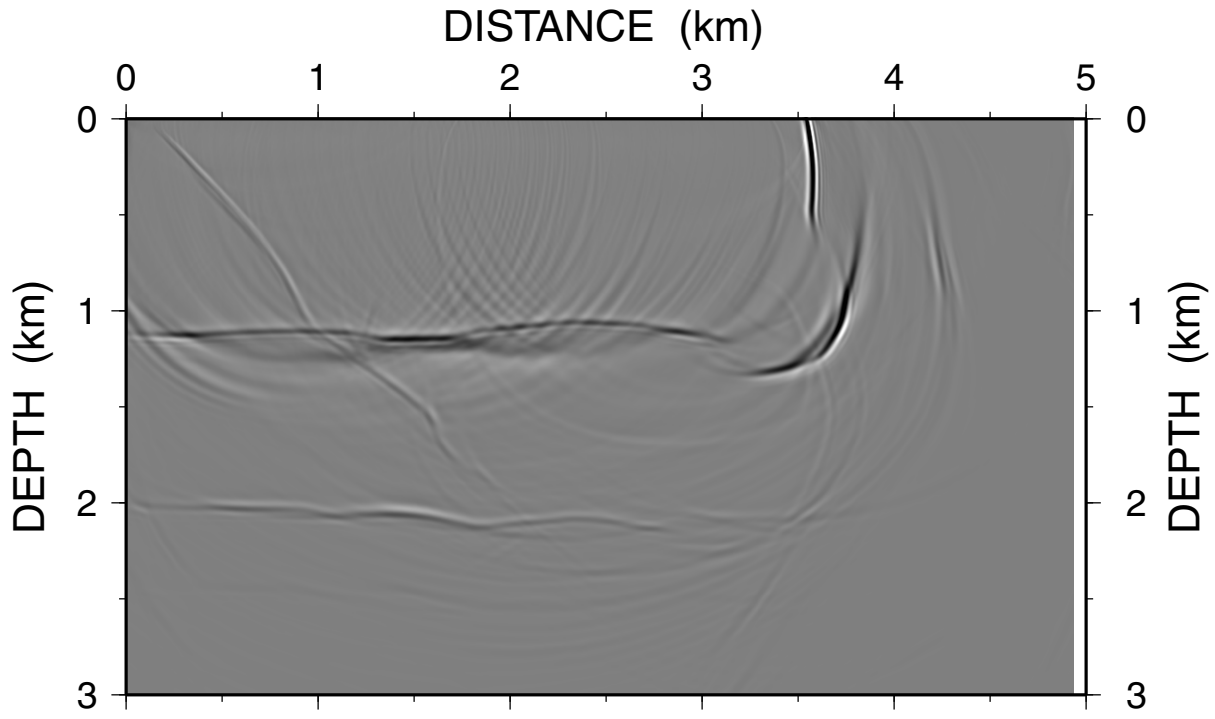

Figure 13. Migration image using velocity model of Figure 7a with all 5 anomalous bodies from Figures 10, 11, and 12 added to simulate tomography errors. The anomalies were increased to 200 m/s in amplitude. All events are easily identified. The 1 km reflector is more smeared than in Figure 8 and the 2 km reflector is undulating. In the upper 1 km, the 45 degree reflector is well imaged, but below 1 km depth, it is more poorly imaged than in Figure 8. The vertical fault is imaged nearly as well as in Figure 8. The gray scale is the same as in Figure 4.

not imaged quite as deep as the tomographic velocity model migration (Figure 8), but its coherence remains excellent. The 45^{o} reflection location has more lateral variation than in Figure 8, but displays strong coherency.

COMMON IMAGE GATHERS

Migrated cross-sections are an adequate way of assessing the quality of the velocity model when the true Earth model is known. However, with real data, the true subsurface is unknown making assessment of results difficult. To check the effectiveness of an iteration of migration and particular velocity model, common image gathers (CIG) or similar plots are utilized. A common image gather is a gather of migrated traces below a fixed surface location. To stack in, an event must be horizontal in the CIG. If it is not, then the lack of horizontality in the CIG is used to update the velocity model through the process of migration velocity analysis (e.g., Lafond and Levander, 1993; Yilmaz and Chambers, 1984). The CIG's were constructed from stacked common-shot gathers instead of the traditional stacked common-offset gathers, because shot gathers were used as input for the migration code. Offset varies systematically with shot number, so the information conveyed is similar.

Standard CIG's as described above were constructed to assess migrated horizontal events. Common-depth CIG's were also constructed to assess steeply dipping features. A migrated shot gather is an X-Z image. A "trace" in a standard CIG is all grid nodes along Z at a chosen fixed X position from a migrated gather. A "trace" in a common-depth CIG is all grid nodes along X at a chosen fixed Z from a migrated gather. X position is plotted horizontally in these common depth slices, so stacking is vertical and events should be vertical to stack in properly. This is an unusual plotting orientation for data, but traditional plotting and sectioning are not always appropriate for steep dips (Levin et al., 1997).

Figure 14 (a-c) shows standard CIG's at X = 1800 m. Reflections are flat from the 1 km and 2 km boundaries for the true velocity model (Figure 14a). There is under-sampling at the edge of the migrated data set and some large amplitude stretching occurs at critical offsets. The 45^{o} dipping event is present at about 1700 m depth. It is flat for a shorter distance due to its dip and resulting smaller aperture of shots that sample this

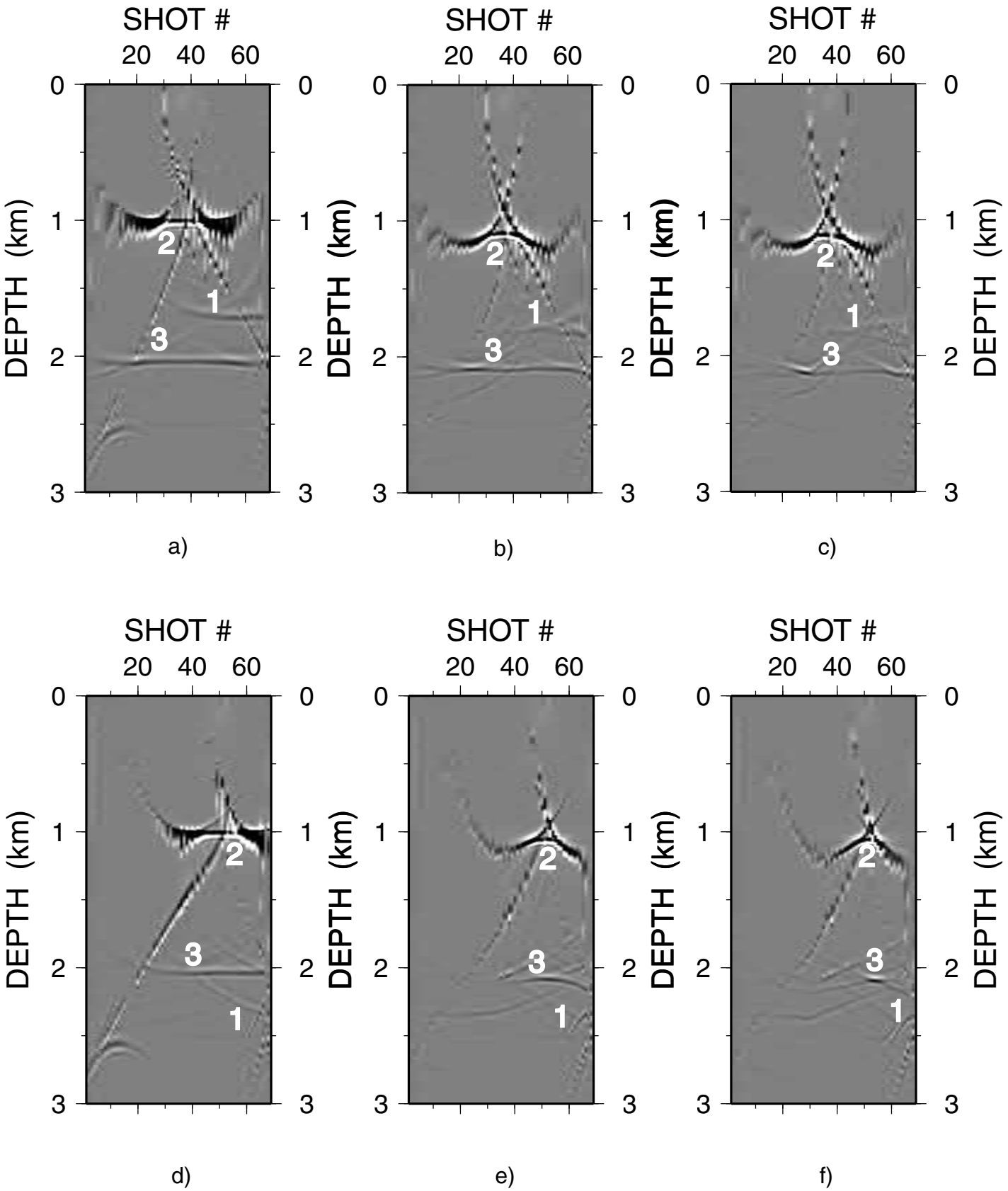

Figure 14. Common image gathers at X = 1800 m (a-c) and X = 2500 m (d-f) for migrations using (a,d) true velocity model (Figure 4), (b,e) velocity model from tomography (Figure 7), and (c,f) tomography velocity model with five anomalies added (Figure 13). '1' is 45 degree dipping fault reflection, '2' is basement reflection from 1 km depth, '3' is reflection from the low velocity zone at 2 km depth.

reflection point. The standard CIG from the migration using the tomographic velocity model (Figure 7a) shows more curvature in the reflectors (Figure 14b). The 45^o dipping and 1 km horizontal events are curved downward at longer offsets, indicating the velocity model is too fast in the deeper portion of the sedimentary basin. By smoothing the refractor and eliminating the resulting first arrival quirks of the migration code in the tomographic velocity model migration, effects near the critical angle are reduced. The 2 km reflector is better migrated than the 1 km reflector, as the average velocity to that depth is approximately correct and the narrower range of angles sampled is less sensitive to errors. Each reflector is still sharply defined, and could be easily picked for further velocity refinement. For noisy data, identification of non-horizontal events requires no spatial aliasing of the data, which assumes dense shot spacing. The event is difficult to pick only at very long offsets where reflections may interfere. These problems would be more difficult to spot on real data gathers, but could be iteratively improved by migration moveout analysis. The reflectors are more variable when anomalous bodies are added to the velocity model (Figure 14c). However, large portions of the reflectors could be confidently picked for velocity model improvement, and thus after several velocity model updates and migrations, the true subsurface model could be recovered.

Figure 14 (d-f) displays a slice through a different portion of the data set, at X = 2500 m, for the same three migration velocity models. The 1 km and 2km events are horizontal for the true velocity model with stretching at long offsets (d). The 1 km and 2 km events behave similarly to the previous case for both (e) and (f). At this point in the data, the 45^o dipping reflection has moved to about 2300 m in depth. It is similar in (a) to the above example, but deteriorates considerably by (b) and is destroyed by (c). This is not surprising given its depth and very long raypaths required to image it.

A common-depth CIG at 400 m (Figure 15) shows how much more unaffected the vertical reflector is to errors in the velocity model. The vertical reflector shows a clean vertical event for shot gathers 30 through 69 for all three velocity models, as does the 45^o event. No geologic dip information is present in these plots, only velocity model errors. Prior to shot gather 30, the vertical fault reflection does not exist. This is caused by either the long distances between shots and the fault, which prohibits the fault from being a first-arrival on the shot gathers, or the first arrival problems mentioned previously. The

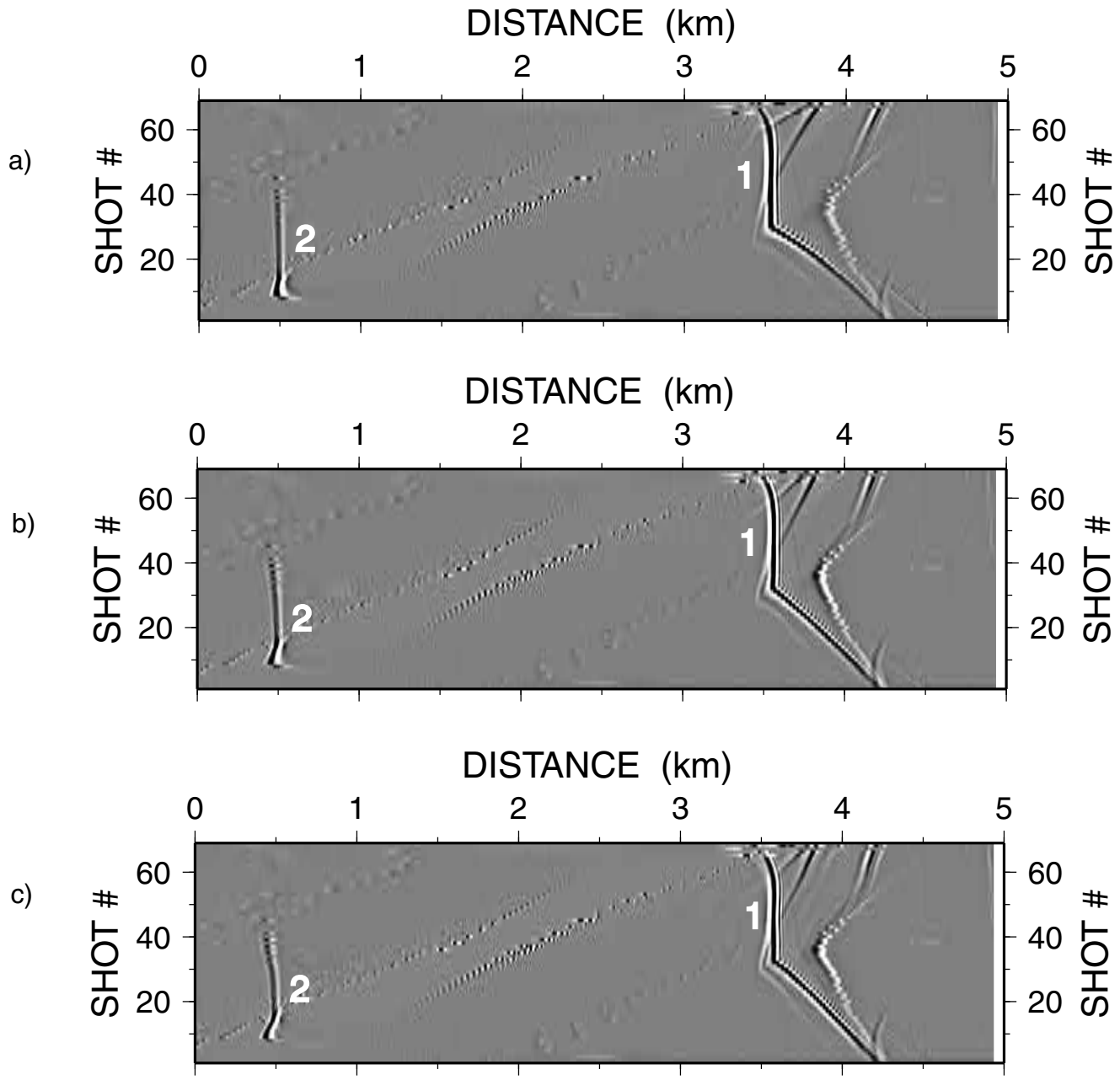

Figure 15. Common-depth Common image gather at Z = 400 m. This unusual plot is described in the text. (a) Migration using true velocity model (Figure 4), (b) velocity model from tomography (Figure 7), and (c) tomography velocity model with five anomalies added (Figure 13). '1' is the vertical fault reflection, '2' is the 45 degree dipping fault reflection.

true velocity model plot displays a sharper and cleaner image than the tomographic velocity model with anomalies added, but even this effect is very minor. The velocity models, as derived from first break traveltime tomography, are well constrained in the shallow portion of the model, where the vertical reflection is important.

DISCUSSION

To efficiently utilize first arrival traveltime tomography as a velocity model building tool for imaging steeply dipping structures, several data acquisition requirements must be met. Densely spaced sources and receivers should be used to increase the subsurface sampling. Non-spatially aliased sources and receivers for the steeply dipping events are required for high migration stacking fold and migration velocity analysis. They also improve the ability to pick first breaks and increase the resolution of the tomography velocity model. In accordance with Snell's Law, a positive velocity gradient is required so that rays return to the surface in tomography. A higher gradient allows deeper sampling at shorter offsets. If the velocity gradient is low and then becomes high at depth, a shadow zone effect will occur. A more energetic source is required so that longer offsets can be recorded and turning rays can sample deeper into the subsurface. However, to capture deep energy, both refracted/turning first breaks and deep steep dip reflections, longer recording times and longer offsets are needed (Stadtlander and Brown, 1997). Longer offsets and larger sources also allow reflections to be recorded from deeper on steeply dipping events by recording reflected energy from further down in the section.

Acquiring longer offsets and using larger sources, while retaining dense spacings will provide for additional costs. However, acquisition parameters for a successful steep-dip migration are very similar to those needed for first arrival traveltime tomography. For instance, to properly relocate energy into its correct subsurface position during migration, adequate recording times and offsets must be used (Lynn and Deregowski, 1981). Also, by principle, the more image points that exist, the better resolved the migrated image. Likewise, for steep dip migration, spatial aliasing is a concern (Yilmaz, 1987). Some planning is required during survey design to ensure that rays for both tomography and steep-dip migration sample the necessary parts of the model. Yet, a data

set acquired for imaging properly with steep-dip prestack depth migration is well suited for first arrival traveltime tomography.

First arrival traveltime tomography can be used to construct a preliminary subsurface velocity model for prestack migration imaging of steep dips. The quality of the migration image depends upon the resolution in a given portion of the tomography velocity model. Resolution of the velocity model is determined by the raypath geometry and density, which, in turn, are governed by the source and receiver geometry and the subsurface velocity model. Isolated anomaly tests were used to demonstrate that the resolution can be markedly different in different portions of the model. Using first arrival traveltimes in the tomography creates issues when triplications are present in the refraction wave field. The secondary arrivals are not picked and subsurface information is lost, creating shadow zones in the model. It was shown that velocity models containing smoothed shadow zones can still produce an image that is sufficient to allow improvement through migration velocity analysis. In poor data areas or underexplored areas, first arrival traveltimes are the only data available to build a migration velocity model. Refraction traveltime tomography can be used for construction of an acceptable velocity model for steep-dip prestack depth migration.

References

Audebert, F., Nichols, D., Rekdal, T., Biondi, B., Lumley, D.E., and Urdaneta, H., 1997, Imaging complex geologic structure with single-arrival Kirchhoff prestack depth migration: Geophysics, **62**, 1533-1543.

Biondi, B., 1990, Velocity estimation by beam stack: field-data results: 60th Ann. Internat. Mtg., Soc. Expl. Geophys., Expanded Abstracts, 1271-1274.

Bording, R.P., Gersztenkorn, A., Lines, L.R., Scales, J.A., and Treitel, S., 1987, Applications of seismic traveltime tomography: Geophys. J. Roy. Astr. Soc., **90**, 285-303.

Eberhart-Phillips, D., and Michael, A.J., 1993, Three-dimensional velocity structure, seismicity, and fault structure in the Parkfield region, central California: J. Geophys. Res., **98**, No. B9, 15,737-15,758.

Fagin, S. W., 1999, Model-based Depth Imaging: Soc. of Expl. Geophys.

Geoltrain, S. and Brac J., 1993, Can we image complex structures with first-arrival traveltime?: Geophysics, **58**, 564-575.

Hale, D., Hill, N.R., and Stefani, J., 1992, Imaging salt with turning seismic waves: Geophysics, **57**, 1453-1462.

Hole, J.A., Thybo, H., Klemperer, S.L., 1996, Seismic reflections from the near vertical San Andreas Fault: Geophys. Res. Lett., **23**, No. 3, 237-240.

Hole, J.A., and Zelt, B.C., 1995, 3-D Finite-difference reflection traveltimes: Geophys. J. Internat., **121**, 427-434.

Hole, J.A., 1992, Nonlinear high resolution three-dimensional seismic traveltime tomography: J. Geophys. Res., **97**, B5, 6553-6562.

Jensen, F.B., Kuperman, W.A., Porter, M.B., and Schmidt, H., 1994, Computational Ocean Acoustics: Springer/American Institute of Physics.

Lafond, C.F., and Levander, A.R., 1995, Migration of wide-aperture onshore-offshore seismic data, central California: seismic images of late stage subduction: J. Geophys. Res., **100**, B11, 22,231-22,243.

Lafond, C.F., and Levander, A.R., 1993, Migration moveout analysis and depth focusing: Geophysics, **58**, 91-100.

Lailly, P., and Sinoquet, D., 1996, Smooth Velocity Models in reflection tomography for imaging complex geologic structures: Geophys. J. Internat., **124**, 349-362.

Lemiszki, P.J., and Brown, L.D., 1988, Variable crustal structure of strike-slip fault zones as observed on deep seismic reflection profiles: Geol. Soc. Amer. Bull., **100**, 665-676.

Levin, S.A., 1998, Resolution in seismic imaging: is it all a matter of perspective?: Geophysics, **63**, 743-749.

Lynn, H.B., and Deregowski, S., 1981, Dip limitations on migrated sections as a function of line length and recording time: Geophysics, **46**, 1392-1397.

MacKay, S., 1990, Depth-focusing analysis and focal surface imaging: A North Sea case history: 60th Ann. Internat. Mtg., Soc. Expl. Geophys., Expanded Abstracts, 1241-1244.

McMechan, G. A., Chang, H., VanDyke, J.P., Solano, M., and Epili, D., 1998, 3-D prestack Kirchhoff depth migration: From prototype to production in a massively parallel processor environment: Geophysics, **63**, 546-556.

Mills G.F., Brzostowski, M.A., Ridgway S., and Barton, C., 1993, A velocity model building technique for prestack depth migration: First Break, **11**, 435-443.

Ratcliff, D.W., Gray, S.H., and Whitmore Jr., N.D., 1992, Seismic imaging of salt structures in the Gulf of Mexico: The Leading Edge, No. 3, 15-31.

Robinson, W.B., 1943, Refraction waves reflected from a fault zone: Geophysics, **1**, 3-8.

Rymer, M. J., Catchings, R.D., Goldman, M.R., Fuis, G.S., Huggins, R., Lippus, C., and Hole, J.A., 1999, Structural complexity in the San Andreas fault zone as revealed by high-resolution seismic reflection and refraction profiling near Parkfield, California. Eos Trans. Amer. Geophys. Union, V 80, Fall Meeting Suppl. F706.

Schultz, P.S., and Sherwood, J.W.C., 1980, Depth migration before stack: Geophysics, **45**, 376-393.

Schneider, W. A., 1978, Integral formulation for migration in two-dimensions and three-dimensions: Geophysics, **43,** 49-76.

Stadtlander, R., and Brown L., 1997, Turning waves and crustal reflection profiling: Geophysics, **62**, 335-341.

Tieman, H. J., 1995, Migration velocity analysis: Accounting for the effects of lateral velocity variations: Geophysics, **60,** no. 01, 164-175.

Unsworth, M.J., Malin, P.E., Egbert, G.D., and Booker, J.R., 1997, Internal structure of the San Andreas fault at Parkfield, California: Geology, **25**, 359-362.

Van Trier, J., 1990, Reflection tomography after depth migration: field data results: 60th Ann. Internat. Mtg., Soc. Expl. Geophys., Expanded Abstracts, 1279-1282.

Versteeg, R.J., 1990, Sensibility of prestack depth migration to the velocity model: 60th Ann. Internat. Mtg., Soc. Expl. Geophys., Expanded Abstracts, 1275-1278.

Vidale, J., 1990, Finite-difference calculation of traveltimes in three dimensions: Geophysics, **55**, 521-526.

Whiting, P., 1998, Tomographic velocity model building for pre-stack depth migration: Expl. Geophys., **29**, 649-653.

Yilmaz, O., 1986, Seismic Data Processing, Investigations in Geophysics No. 2: Soc. Expl. Geophys.

Yilmaz, O. and Chambers, R. E., 1984, Migration velocity analysis by wave-field extrapolation: Geophysics, **49,** no. 10, 1664-1674.

Zelt, B.C., Talwani, M. and Zelt, C.A., 1998, Prestack depth migration of dense wide-angle seismic data: Tectonophysics, **286**, 193-208.

Zelt, C.A., 1999, Modeling strategies and model assessment for wide-angle seismic traveltime data: Geophys. J. Internat., **139**, 183-204.

Zhang, J., and Toksoz, M.N., 1998, Nonlinear refraction traveltime tomography: Geophysics, **63**, 1726-1737.

Zhao, P., Uren, N.F., Wenzel, F., Hatherly, P.J., and McDonald, J.A., 1998, Kirchhoff diffraction mapping in media with large velocity contrasts: Geophysics, **63**, 2072-2081.

Zhuand, J. and Lines, L., 1999, Comparison of Kirchhoff and reverse-time migration methods with applications to prestack depth imaging of complex structures: Soc. Expl. Geophys.

Appendix 1

Kirchhoff prestack depth migration code

The prestack Kirchhoff migration code was written by Dr. David Okaya at the University of Southern California, was used in this study. It was provided to Dr. John Hole to be used in his research.

The source code, the executable, and all associated libraries and support files can be accessed from most of the workstations in the Virginia Tech Geophysical computing center.

…/bin contains the executable file called **kirch2B.**

Another program located here is called **kirchvelprep.** It is used to condition a binary velocity model that is ordered in z-fast to one ordered in x-fast.

…/src contains the source code for both of the above programs, as well as numerous subroutines

…/lib contains the many libraries called by the code

The input velocity model should be in binary format; the output from the tomography code of Hole is already in the correct format for the migration code, there is no need to run kirchvelprep.

The input seismic data should be in SEG-Y format with appropriate headers, input data can be a trace, a shot gather, or a series of shot gathers.

These shot gathers should be in a consistent coordinate system with that of the velocity model. If they are not, modify the SEG-Y headers using seismic UNIX or other utility

The trace headers must contain source/receiver locations. All other optional header values can be specified in the code parameters.

The input velocity model can be a constant velocity or a gridded velocity model (i.e. output from tomography)

It is best to create a script to run **kirch2B,** so that parameters don't have to be re-keyed for each migration run, and for flexibility in running the code.

An example of a script for running the code can be found under …/**bin**
The name of the script is kirch2b.com.

kirch2B will self-document if no command line arguments are specified. It will provide the user with all available parameters. Command line arguments not in square or curly brackets are mandatory. Arguments in square brackets are optional and usually have default values. Arguments in curly brackets are in a set; two sets of curly brackets are either/or.

Input data is expected to be rectangular in receivers/shots (ng * ns). Seismogram description (nt= dt=) is mandatory. Decimation of input traces is possible using s0= s1= ds= g0= g1= dg=. By default, all input seismic data are used. If data is reduced, provide vred= t0=. Source/receiver elevations are read from standard SEG-Y header locations unless otherwise specified by bsx= bsy= brx= bry= bsz= brz=.

If an input velocity file is going to be used, specify vel= nx= nz= h=. If the velocity model is 3-D, specify ny=. For a constant velocity migration, specify velconst=. Size of constant velocity model is determined from xM0= xM1= zM0= zM1= yM0= yM1=. Regardless of velocity model used, input grid coordinate of first corner by velx0= vely0= velz0=.

Downward traveltime fields can be output during migration by specifying timeQC=ishot,ichan

Migration parameters can also be controlled. Dip limits can be placed in code by specifying cutoff=. If no cutoff is specified, Kirchhoff ellipse to surface will be migrated. A taper on the migrated ellipse can also be specified through taper=. A selected offset range can be processed using offset0= offset1=. Trace muting can also be applied uniformly, before migration by specifying unredmutet0= unredmutet1=. The length of the taper is taperT=.

The image can be output in a number of ways. Image= partialgath= bytrace= are all output forms, and at least one must be specified. The output depth volume must be described using x0= x1= z0= z1=. The grid sizes must also be specified through dz= and dx=.

Output format can be SEG-Y, Sierra SEG-Y, or binary. An already created image can be added to using sumimage=. An already existing partial image file can be added to using appendimage=. Migrated images can be saved every delimage= # traces.

A world-wide-web documentation of the code and a brief synopsis is available in …/**okaya** or may be available at http://earth.usc.edu/~okaya/progs/kirch/kirch2B.html.

Appendix 2

First-Arrival Traveltime Tomography Code

Input traveltime data are first arrivals picked using FOCUS or other application.

A velocity model must be created for use as input into the tomography codes. This can be created using the program *vel1d*, which creates a 1-D velocity model. The source code can be found under /haida/hole/src. A parameter file is used as input for the program. For an example of this parameter file, go to /haida/hole/…

Survey geometry is defined through two geometry files that will be located in a subdirectory of the tomography directory called **geom**. One file will be for the sources and one file will be for the receivers. The receiver file should contain at least 5 columns: line number, receiver #, X, Y, Z, and an optional column of time statics. The shot file contains the columns: shot number, X, Y, Z. The picks files should contain the receiver number, two columns of zero, and a column containing the traveltimes to those receivers from a particular shot. There are several nawk scripts that should help in sorting traveltime picks and the geometry files.

The pick files are to be placed in a subdirectory of the tomography directory called **pix.** These will be used by the three main programs to do the tomography. An example of these pick files exists under /haida/hole/park/../.

In the tomography directory, there should be a file called **set.h**. This is the most important file for keeping organization in the tomography. It contains all necessary information about locations of files, array sizes, etc. It is essential to make sure this file points to all the correct locations for the pick files, the geometry files, and the velocity model.

Once this file is created, there are a few make files that need to be ran to set up the code for the individual parameters chosen. These make files can be found under /haida/hole/../. There are several parameters in these make files that may need to be changed before tomography can be run. They need to be executed in a specific order, so that no files are missing.

The picks and the geometry, as well as the set.h file need to be created first. These files will be called by most all the make files. The make files include mkpar.com, mkpcov.com, mktomdu.com. mkpar.com creates a subdirectory of the tomography directory called **par.** In this directory are parameter files for punch and cover, the two codes that actually perform the tomographic inversion.

Once the make files have created the scripts to properly run the code for your setup, the code can be executed through another script called runfull.com. Runfull.com contains all the parameters that are interactively input into the programs pucov.com, tomdu.com, and punch.

Punch is the Eikonal solver forward modeling program used to trace the raypaths through the velocity model.

The velocity model is created before running runfull.com. The velocity model must be moved to the run subdirectory before execution of the program.

Before running tomography, make sure there are picks at every receiver, for every shot. Make sure there are parameter files for every shot, located in the **par** subdirectory. Make sure pucov.com and tomdu.com are located in the tomography directory, as well as the set.h file. Make sure the rec and shot geometry files are located in the **geom** subdirectory. Make sure a **run** subdirectory exists and runfull.com and a vel.3d file are located within this directory. Make sure runfull.com is pointing to all the correct directories and files.

Again, examples of all of these files exists in a number of places, including /elk/bcarney/tomog -- /elk/bcarney/tomogsynth -- /haida/bcarney/park/tomogsynth -- /haida/hole/pub/tomography -- /haida/hole/tomog/parkfield. One or more of these places will have examples of all files.

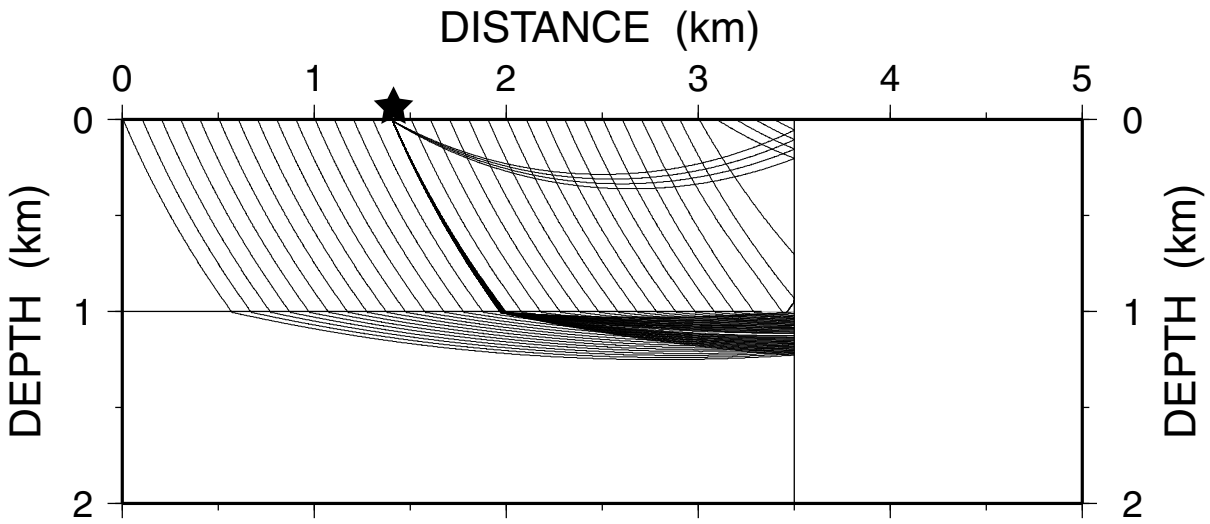

Figure A1. Reflected raypaths from vertical fault for shot at X = 1407 m, designated by a star. The dark line coming directly from the shot down to the 1 km interface represents a large number of rays that are refracted into the basement as head waves. These rays have a smaller amplitude than rays that turn in the basin. Notice that sedimentary basin turning rays are only first arrivals down to about 250 m. Below this, they are secondary arrivals that are not modeled correctly in the migration.

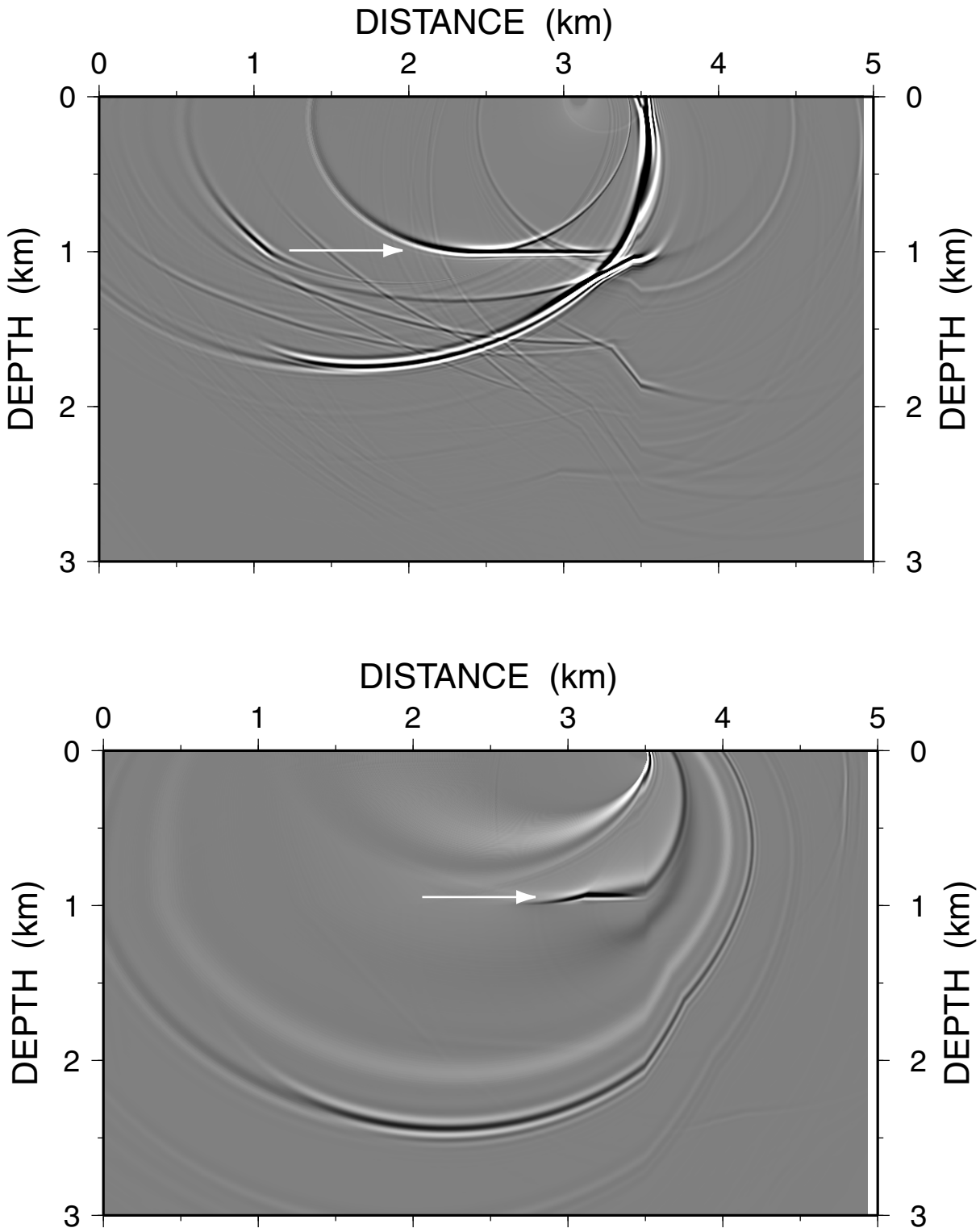

Figure A2. Migrated shot gathers at X = 2900 m (top) and X = 3300 m (bottom). These gathers prove that energy does exist at the 1 km boundary all the way to the fault. However, notice on the top figure that the energy is masked beginning at about X = 3300 m. Only shot gathers between X = 3300 m and the vertical fault will provide energy very close to the fault for the migrated image making it a very small event.

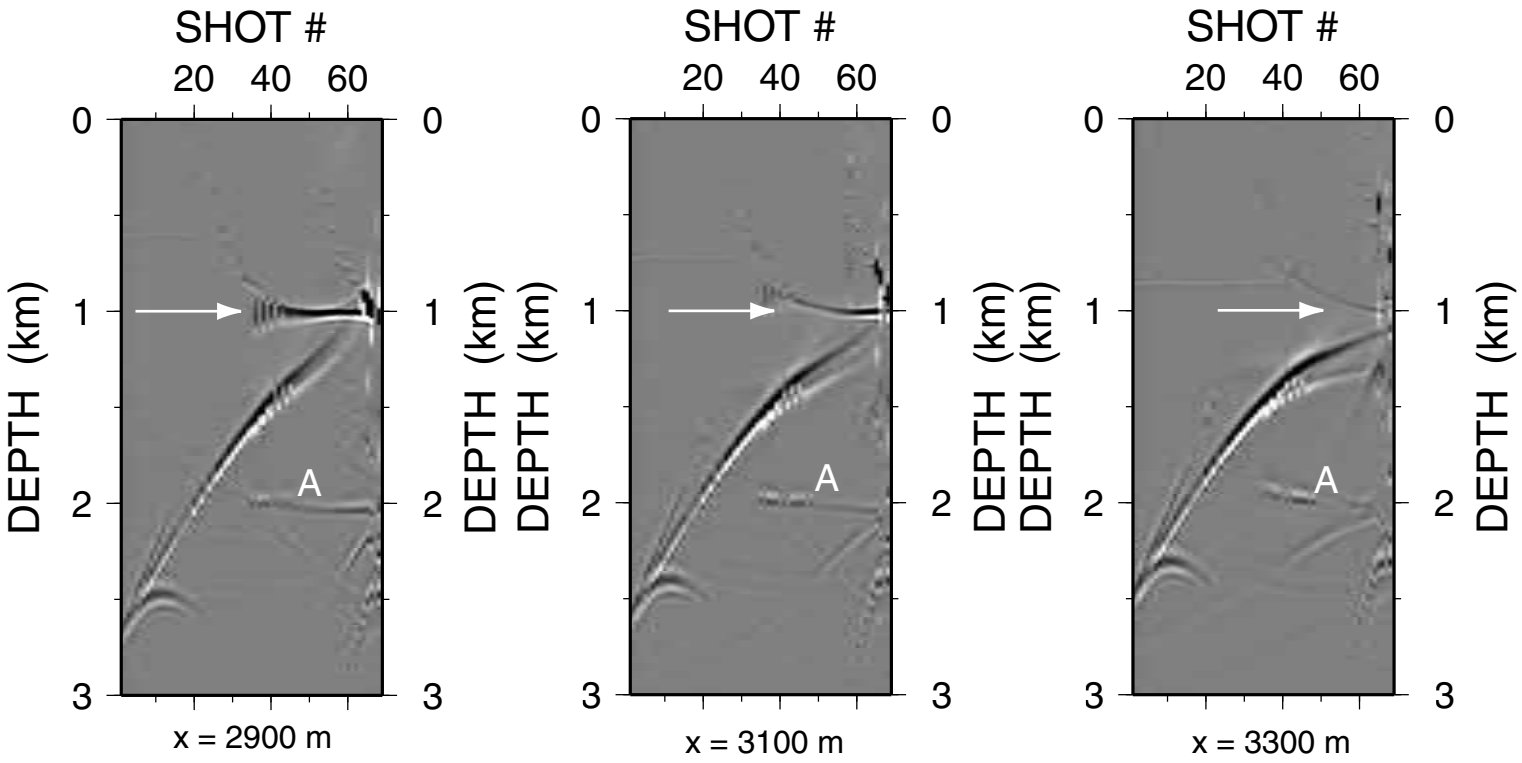

Figure A3. Three common image gathers at X = 2900 m, X = 3100 m, and X = 3300 m displaying effect of losing the 1 km basement reflection as it nears the vertical fault. Due to only using shots to the left of the vertical fault for migration, the fold of the data decreases rapidly toward the fault. This coupled with pre-migration muting cancels out most of the energy from the 1 km reflector, as is denoted by the white arrow in the figure above. 'A' denotes location of the 2 km low velocity zone.

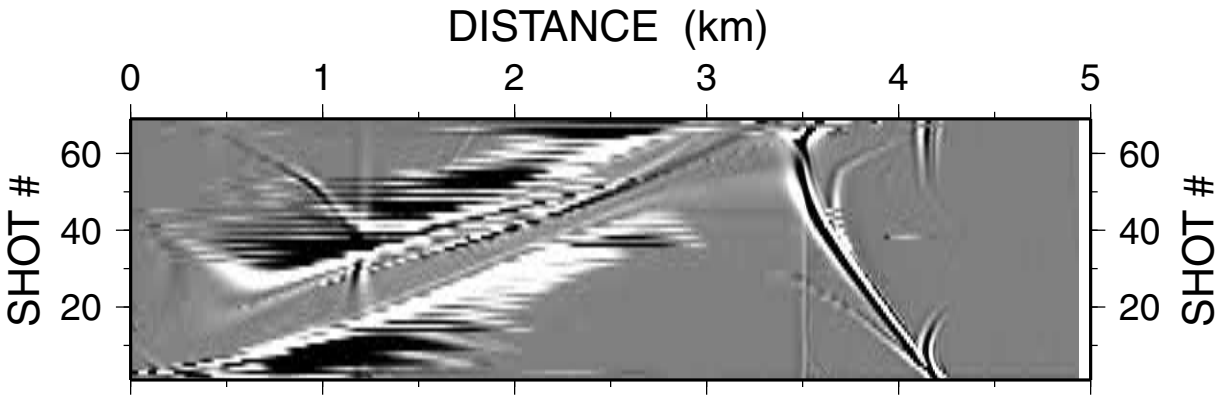

Figure A4. Common-depth common image gather at Z = 1100 m from true velocity model (Figure 1) migrated data. The vertical fault reflector is present at this depth even though it is below ambient noise in the migrated section (Figure 4). The event beginning at approximately X = 3 km and curving to the right going from shot 69 to shot 1 is the reflected refraction from the vertical fault at approximately 1.1 km depth. The event is not vertical due to the first arrival to the fault at this location being a refraction into the basement instead of a reflection from the vertical fault.

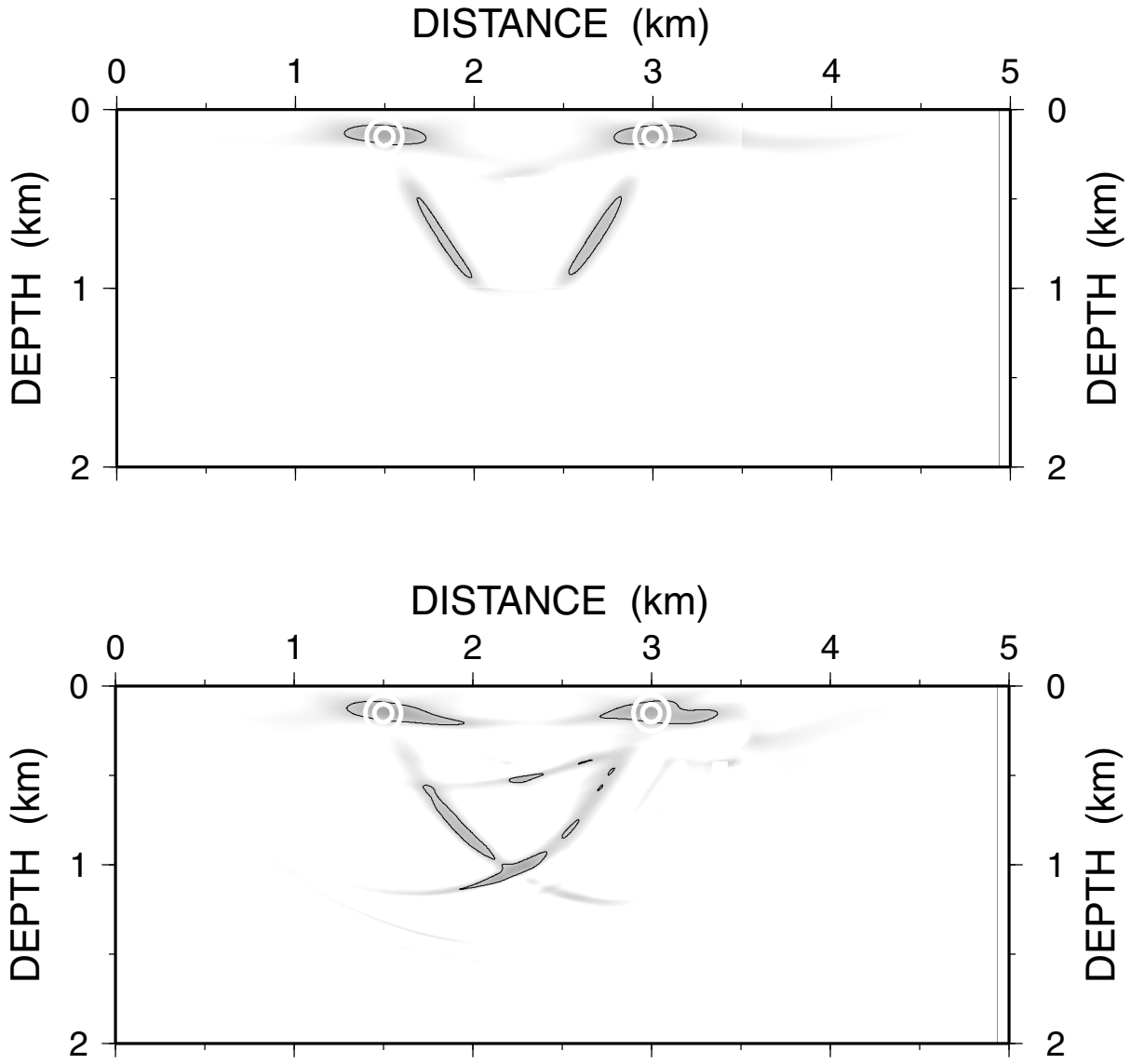

Figure A5. Plots similar to Figure 10, but for two 50 m anomalies added to the velocity model in Figure 1. White circles show one and two spatial standard deviation (50 m) locations for the anomalies. (a) tomography result using a starting model equal to Figure 1 and subtracting Figure 1 for the plot. (b) tomography result using same starting model as in Figure 7 (constant velocity gradient) and subtracting model in Figure 7a for the plot. The maximum anomaly value is 12 m/s, and the contour interval is 8 m/s. This test is demonstrative of anomaly sizes just below the resolution limit. The anomalies have been smeared significantly and their amplitudes are diminished.

Vitae

Brooke J. Carney received his Bachelor of Science degree from Virginia Tech in 1998. He is the first person to complete his studies in the 5 year BS/MS program in the Department of Geological Sciences. He will continue to perform the work of a geophysicist at Marathon Oil Company in Oklahoma City, Oklahoma.